New Journal of Physics
The open–access journal for physics

Scaling and formulary of cross-sections for ion–atom impact ionization

Igor D Kaganovich, Edward Startsev and Ronald C Davidson
Plasma Physics Laboratory, Princeton University, Princeton, NJ 08543, USA
E-mail: ikaganov@pppl.gov

New Journal of Physics **8** (2006) 278
Received 5 April 2006
Published 28 November 2006
Online at http://www.njp.org/
doi:10.1088/1367-2630/8/11/278

Abstract. The values of ion–atom ionization and stripping cross-sections are frequently needed for many applications that utilize the propagation of fast ions through matter. When experimental data and theoretical calculations are not available, approximate formulae are frequently used. This paper briefly summarizes the most important theoretical results and approaches to cross-section calculations in order to place the discussion in historical perspective and offer a concise introduction to the topic. Based on experimental data and theoretical predictions, a new fit for ionization cross-sections is proposed. The range of validity and accuracy of several frequently used approximations (classical trajectory, the Born approximation, and so forth) are discussed using, as examples, the ionization cross-sections of hydrogen and helium atoms by various fully stripped ions. A formulary of analytical approximations for cross-sections is presented.

PII: S1367-2630(06)22088-3

Contents

1. Introduction

Ion–atom ionizing collisions play an important role in many applications such as heavy ion inertial fusion [1], collisional and radiative processes in the Earth's upper atmosphere [2], ion-beam lifetimes in accelerators [3], atomic spectroscopy [4], and ion stopping in matter [5], and are of considerable interest in atomic physics [6]. The recent resurgence of interest in charged particle beam transport in background plasma is brought about by the recognition that plasma can be used as a magnetic lens. Applications of the plasma lens ranging from heavy ion fusion to high energy lepton colliders are discussed in [6]–[10]. In particular, both heavy ion fusion and high energy physics applications involve the ion transport in plasmas and gases: partially stripped heavy elements for heavy ion fusion; positrons for electron–positron colliders [9]; and high-density laser-produced proton beams for the fast ignition of inertial confinement fusion targets [11].

To estimate the ionization and stripping rates of fast ions propagating through gas or plasma, the values of ion–atom ionization cross-sections are necessary. In contrast to the electron [12] and proton [13]–[15] ionization cross-sections, where experimental data or theoretical calculations exist for practically any ion and atom, the knowledge of ionization cross-sections by fast complex ions and atoms is far from complete [16]–[19], [20]. When experimental data and theoretical calculations are not available, approximate formulae are frequently used.

The *raison d'etre* of this paper are the frequent requests that we have had from colleagues for a paper describing the regions of validity of different approximations and scaling laws

in the calculation of ion–atom ionization and stripping cross-sections. The experimental data on stripping cross-sections at low projectile energy were collected in the late 1980s, while comprehensive quantum-mechanical simulations were performed in the late 1990s. Having in hand both new experimental data and simulation results enabled us to identify regions of validity of different approximations and propose a new scaling law, which is the subject of the present paper.

The most popular formula for ionization cross-sections was proposed by Gryzinski [21]. The web of science search engine [22] shows 457 citations of the paper, and most of the citing papers use Gryzinski's formula to evaluate the cross-sections. In this approach, the cross-section is specified by multiplication of a scaling factor and the unique function of the projectile velocity normalized to the orbital electron velocity. The popularity of Gryzinski's formula is based on the simplicity of the calculation, notwithstanding the fact that his formula is not accurate at small energies.

Another fit, proposed by Gillespie, gives results close to Gryzinski's formula at large energies, and makes corrections to Gryzinski's formula at small energies [23]. Although more accurate, Gillespie's fit is not frequently used in applications, because it requires a knowledge of fitting parameters not always known a priori.

In [24], we have proposed a new fit formula for ionization cross-section which has no fitting parameters. The formula is checked against available experimental data and theoretical predictions. In the present paper, we compare this scaling formula for impact-ionization cross-sections with a much broader selection of experimental results. Note that previous scaling laws either used fitting parameters or actually did not match experiments for a wide range of projectile velocities. We also briefly review the most important theoretical results and approaches to cross-section calculations in order to place the discussion in historical perspective and offer non-specialists a concise introduction to the topic. The advantages and limitations of two most widely used approximations—the classical mechanical calculations and the Born approximation of quantum mechanics—are reviewed.

The organization of this paper is as follows. In section 2 we give a brief overview of key theoretical results and experimental data. Further details of the theoretical models are presented in appendices. The new proposed fit formula for ionization cross-section is presented at the end of section 2, including a detailed comparison with experimental data, and in section 3 a short summary of theoretical approaches and their limitations is presented. Finally, a formulary of analytical approximations for cross-sections and their limitations is presented in section 4 for reference purposes.

2. Overview of experimental data and proposed scaling laws for ionization cross-sections

There are several theoretical approaches to cross-section calculations. These include: classical calculations that make use of a classical trajectory and the atomic electron velocity distribution functions (EVDFs) given by quantum mechanics (this approach is frequently referred to as classical trajectory Monte Carlo (CTMC)); quantum-mechanical calculations based on Born, eikonal or quasi-classical approximations, and so forth [16]–[19], [20]. All approaches are computationally intensive and the error and range of validity are difficult to estimate in most cases. Therefore, different fittings and scalings for cross-sections are frequently used in practical applications.

Most scalings were developed using theories and simulations based on classical mechanics. Classical trajectory calculations are easier to perform compared with quantum-mechanical calculations. Moreover, in some cases the CTMC calculations yield results very close to the quantum-mechanical calculations [25]–[28]. The reason for similar results lies in the fact that the Rutherford scattering cross-section is identical in both classical and quantum-mechanical derivations [29]. Moreover, the ionization probabilities for hydrogen-like orbitals calculated in the quantum mechanical and classical mechanical approaches are very similar, as shown in appendix B (see figure B.2). Therefore, when an ionizing collision is predominantly a consequence of the electron scattering at small impact parameters close to the nucleus, the quantum mechanical uncertainty in the scattering angle is small compared with the angle itself, and the classical calculation can yield an accurate description [30]–[32]. Whereas in the opposite limit, when an ionizing collision is predominantly a consequence of the electron scattering at large impact parameters far from the nucleus, the quantum-mechanical uncertainty in the scattering angle is large compared with the angle itself, and the classical calculation can remarkably fail in computing the ionization and stripping cross-section [33, 34]. Similarly, the Born approximation can grossly overestimate the cross-sections if the transition probability is not small and the Born approximation is not valid.

In the present analysis, we consider first the ionization cross-section of the hydrogen-like electron orbitals (for example one-electron ions), with nucleus of charge Z_T, colliding with a fully stripped ion of charge Z_p. Subsequently, we show that the approach can be generalized with reasonable accuracy for any electron orbital, making use of the ionization potential of the electron orbitals. Because different terminology is used in the literature, we call a *stripping collision* a collision in which the fast ion loses an electron in a collision with a stationary target ion or atom (in the laboratory frame); and we call an *ionizing collision* a collision in which a fast ion ionizes a stationary target ion or atom [16]. Both cases are physically equivalent to each other by changing the frame of reference, and further consideration can be given in the frame of the atom or ion being ionized. In accelerator applications, the electron stripping from the accelerated ions usually occurs due to collisions with neutral atoms of residual gas, because the gas density is larger than the plasma density. However, in heavy ion fusion or high energy density physics applications, the interaction of intense ion beams with a background plasma is becoming increasingly important, where electron stripping occurs due to collisions with the ions.

Atomic units are used throughout this paper with $e = \hbar = m_e = 1$, which corresponds to length normalized to $a_0 = \hbar^2/(m_e e^2) = 0.529 \times 10^{-8}$ cm, velocity normalized to $v_0 = e^2/\hbar = 2.19 \times 10^8$ cm s^{-1}, energy normalized to $E_0 = m_e v_0^2 = 2$ Ry $= 27.2$ eV, where Ry is the Rydberg energy. The normalizing coefficients are kept in all equations for robust application of the formulae. For efficient manipulation of the formulae it is worth noting that the normalized projectile ion velocity is $v/v_0 = 0.2\sqrt{E[\text{keV amu}^{-1}]}$, where E is energy per nucleon in keV amu^{-1}. Therefore, 25 keV amu^{-1} corresponds to the atomic velocity scale. Some papers express the normalized velocity v/v_0 as $\beta\alpha$, where $\beta = v/c$, and $v_0/c = \alpha = 1/137$. Here, c is the speed of light, and α is the fine structure constant.

For a one-electron ion, the typical scale for the electron orbital velocity is $v_{nl} = v_0 Z_T$. Here, n, l is the standard notation for the main quantum number and the orbital angular momentum [29]. The collision dynamics is very different depending on whether v is smaller or larger than v_{nl}.

If $v \gg v_{nl}$, the electron interaction with the projectile ion occurs for a very short time and the interaction time decreases as the velocity increases. Therefore, the ionization cross-section

also decreases as the velocity increases. In the opposite case $v \ll v_{nl}$, the electron circulation around the target nucleus is much faster than the interaction time, and the momentum transfer from the projectile ion to the electron averages out due to the fast circulation. Thus, the cross-section decreases as the projectile velocity decreases. This is why the cross-section typically has a maximum at $v = v_{\max} \sim v_{nl}$, but as we shall see below, $v_{\max}$ also depends on the charge of the projectile. The description of cross-sections in the limiting cases of very high and very low velocities can be significantly simplified. Historically, the study of cross-sections started in the beginning of 20th century and proceeded with refinements until the present as can be seen in the following historical overview.

2.1. Behaviour of cross-sections at large projectile velocities $v \gg v_{nt}$

2.1.1. Thompson's treatment. In the first treatment, Thompson calculated the ionization cross-section in the limit $v \gg v_{nl}$ [35]. This treatment neglected completely the orbital motion of the target electrons and assumed a straight-line trajectory of the projectile. In this approximation, the velocity kick acquired by the electron during the collision is entirely in the direction perpendicular to the ion trajectory, because the final action of the force along the trajectory cancels out due to symmetry, i.e., the electron velocity change during the approaching phase is equal to minus the electron velocity change during the departing phase. The momentum acquired by the electron ($m_e \Delta v$) from passing-by projectile moving with the speed v and impact parameter ρ is given by the integral over time of the force perpendicular to ion trajectory $F_\perp = e^2 Z_p \rho / (\rho^2 + v^2 t^2)^{3/2}$, where $t = 0$ corresponds to the distance of the closest approach. Time integration of the force yields

$$\Delta v(\rho) = \frac{2e^2 Z_p}{m_e v \rho}. \tag{1}$$

From equation (1) it follows that only collisions with sufficiently small impact parameters result in ionization. The minimum impact parameter for ionization of an initially stationary electron ($\rho_{\min}$) is $m_e \Delta v(\rho_{\min})^2/2 = I_{nl}$. During a collision with impact parameter $\rho_{\min}$ the energy transfer from the projectile to the electron is equal to the ionization potential $I_{nl} = Z_T^2 E_0/2$, or $\Delta v(\rho_{\min}) = v_{nl}$. Substitution of equation (1) gives the total ionization cross-section $\pi \rho_{\min}^2$ [30, 35]

$$\sigma^{\text{Bohr}}(v, I_{nl}, Z_p) = 2\pi Z_p^2 a_0^2 \frac{v_0^2 E_0}{v^2 I_{nl}}. \tag{2}$$

Similarly, equation (2) can be derived by averaging the Rutherford cross-section over all scattering angles leading to ionization. Although the first derivation of equation (2) was done by Thompson [35] the formula is frequently referred to as the Bohr formula [16].

As shown in following, taking finite orbital electron velocity into account gives a cross-section which is about 5/3 times larger than the Bohr formula in equation (2). This is a consequence of the fact that for an electron with nonzero velocity less energy transfer is required for ionization.

2.1.2. Gerjuoy's treatment. The following treatments account for the effect of finite electron orbital velocity. The most complete and accurate calculations were done by Gerjuoy [36].

He calculated the differential cross-section $\mathrm{d}\sigma/\mathrm{d}\Delta E(v_e, v, \Delta E)$ of energy transfer ΔE in the collision between the projectile ion and a free electron (the target atomic potential was neglected) with given initial speed v_e (and arbitrary direction), by averaging the Rutherford cross-section over all orientations of electron orbital velocity $\mathbf{v}_e$. The total cross-section is then calculated by integration over the energy transfer for energies larger than the ionization potential, and weighted by the EVDF $f(v_e)$. This gives

$$\sigma(v, I_{nl}, Z_p) = Z_p^2 \int_0^\infty \sigma_{I_{nl}}(v, v_e) f(v_e)\, \mathrm{d}v_e, \tag{3}$$

where

$$\sigma_{I_{nl}}(v, v_e) = \int_{I_{nl}}^\infty \frac{\mathrm{d}\sigma}{\mathrm{d}\Delta E}(v, v_e, \Delta E)\, \mathrm{d}\Delta E. \tag{4}$$

A rather complicated analytical expression for $\mathrm{d}\sigma/\mathrm{d}\Delta E(v_e, v, \Delta E)$ is given in appendix A. For large projectile ion velocities ($v \gg v_{nl}$), the differential cross-section can be expressed as [36]

$$\frac{\mathrm{d}\sigma^{\text{high-energy}}_{\text{classical}}}{d\Delta E}(v, v_e, \Delta E) = 2\pi a_0^2 \frac{E_0^2}{\Delta E^3 m_e v^2}\left(\frac{2m_e v_e^2}{3} + \Delta E\right). \tag{5}$$

Substituting equation (5) into equations (3) and (4) gives

$$\sigma^{\text{high-energy}}_{\text{classical}}(v, I_{nl}, Z_p) = \tfrac{5}{3} B_{nl} \sigma^{\text{Bohr}}(v, I_{nl}, Z_p), \tag{6}$$

$$B_{nl} \equiv \frac{3}{5}\left(\frac{2K_{nl}}{3I_{nl}} + 1\right), \tag{7}$$

where σ^{Bohr} is given by equation (2), and $K_{nl} \equiv \langle m_e v_e^2/2\rangle_{nl}$ is the average orbital electron kinetic energy. For hydrogen-like electron orbitals, the average electron kinetic energy is equal to the ionization potential $K_{nl} = I_{nl}$ [29], and $B_{nl} = 1$. The B_{nl} factors are introduced to account for the difference in the EVDFs from the EVDF of the hydrogen-like electron orbitals. The data for K_{nl} are calculated for many atoms in [37]. For example, the average kinetic energy for the helium atom is $K_{nl} \equiv \langle m_e v_e^2/2\rangle = 1.43E_0$, whereas $I_{nl} = 0.91E_0$, and therefore $B_{\text{He}} = 1.22$.

Taking finite orbital electron velocity into account gives a cross-section which is about 5/3 times larger than the Bohr formula in equation (2). This is a consequence of the fact that for an electron with nonzero velocity less energy transfer is required for ionization. To calculate K_{nl} the EVDF can be obtained from a microcanonical ensemble.

Classical mechanics gives the EVDF as a microcanonical ensemble, where

$$f(v_e) = C v_e^2 \int \delta\left(\frac{m_e v_e^2}{2} - \frac{Z_T}{r} + I_{nl}\right) r^2\, \mathrm{d}r. \tag{8}$$

Here, C is a normalization constant defined so that $\int f(v_e)\, \mathrm{d}v_e = 1$, and $\delta(\ldots)$ denotes the Dirac delta-function. Interestingly, the EVDF for a one-electron ion is identical in both the

quantum-mechanical and classical calculations [29, 37] with

$$f(v_e) = \frac{32 v_{nl}^5}{\pi} \frac{v_e^2}{[v_e^2 + v_{nl}^2]^4}, \tag{9}$$

where v_{nl} is the scale of electron orbital velocity

$$v_{nl} = v_0 \sqrt{2 I_{nl}/E_0}. \tag{10}$$

Although a microcanonical distribution provides the same velocity distribution as in quantum theory for hydrogen-like shells, this is not the case for other electron shells. Moreover, the spatial distribution of the charge density is poorly approximated even for hydrogen, vanishing identically for $r > 2a_0$ rather than decreasing exponentially [18]. Substituting the general differential cross-section $\mathrm{d}\sigma/\mathrm{d}\Delta E(v_e, v, \Delta E)$ from equation (A.3) of appendix A and the EVDF in equation (9) into equation (3) yields

$$\sigma^{\mathrm{GGV}}(v, I_{nl}, Z_p) = \pi a_0^2 Z_p^2 \frac{E_0^2}{I_{nl}^2} G^{\mathrm{GGV}}\left(\frac{v}{v_{nl}}\right). \tag{11}$$

Here, the scaling function $G^{\mathrm{GGV}}(x)$ is given by equation (A.10) in appendix A. Approximate formulae are presented in equation (66) using the tabulation of the function $G(x)$ presented in [38] for $x > 1$, and in [39] for $x < 1$. The notation GGV stands for the classical trajectory calculation in equation (66) due to Gerjuoy [36] using the fit of Garcia and Vriens [38].

2.1.3. Bethe's treatment. The classical calculations underestimate the cross-sections for very high projectile velocities $v \gg v_{nl}$. The scattering angle of the projectile due to collision with the target atom is of order $\theta_c = \Delta p/Mv$, where Δp is the momentum transfer in the collision, and M is the mass of the projectile particle. The minimum energy transfer from the projectile is determined by the ionization potential, with $\Delta E = v\Delta p > I_{nl}$ and $\Delta p > \Delta p_{\min} \equiv I_{nl}/v$. Here, we use the fact that the momentum transfer Δp is predominantly in the direction perpendicular to the projectile velocity. The projectile particle with wave vector $k = Mv/\hbar$ undergoes diffraction on the object of the target atomic size a_{nl} with the diffraction angle of order $\theta_d = 1/(ka_{nl}) = \hbar/(Mva_{nl})$ [30]. At large projectile velocities $v \gg v_{nl}$, it follows that $\Delta p_{\min} \equiv I_{nl}/v \ll \hbar/a_{nl}$, because $v_{nl} = I_{nl}a_{nl}/\hbar$ for hydrogen-like electron orbitals. And for small $\Delta p \sim \Delta p_{\min}$, it follows that $\theta_c = \Delta p/Mv \ll \theta_d = \hbar/(Mva_{nl})$. Therefore, the collision cannot be described by classical mechanics in the limit $v \gg v_{nl}$.

Bethe made use of the Born approximation of quantum mechanics to calculate cross-sections [40] (see appendix B for details). This yields for $v \gg v_{nl}$

$$\sigma^{\mathrm{Bethe}} = \sigma^{\mathrm{Bohr}}(v, I_{nl}, Z_p)\left[0.566 \ln\left(\frac{v}{v_{nl}}\right) + 1.261\right]. \tag{12}$$

If the projectile speed is much larger than the electron orbital velocity $v \gg v_{nl}$, the logarithmic term on the right-hand side of equation (12) contributes substantially to the cross-section, and as a result the quantum-mechanical calculation in equation (12) gives a larger cross-section than the classical trajectory treatment in equation (6). The quantum-mechanical cross-section is larger than the classical trajectory cross-section due to the contribution of large impact parameters (ρ) to

the quantum-mechanical cross-section, where the ionization is forbidden in classical mechanics because the energy transfer calculated by classical mechanics is less than the ionization potential ($\Delta E = v\Delta p_c(\rho) < I_{nl}$, where Δp_c is the momentum transfer given by classical mechanics in equation (1)). However, ionization is possible due to diffraction in quantum mechanics [41]. Moreover, integration over these large impact parameters where the ionization is forbidden in classical mechanics, contributes considerably to the total ionization cross-section (see appendix B for further details).

2.1.4. Gryzinski's treatment. Gryzinski attempted to obtain the ionization cross-sections using only classical mechanics similarly to Gerjuoy. But in order to match the asymptotic behaviour of the Bethe formula in equation (12) at large projectile velocities, Gryzinski assumed an artificial EVDF instead of the correct EVDF in equation (9) [21], i.e.,

$$f^{\mathrm{Gryz}}(v_e) = \frac{1}{v_{nl}}\left(\frac{v_{nl}}{v_e}\right)^3 \exp\left(-\frac{v_{nl}}{v_e}\right). \tag{13}$$

The ionization cross-section was calculated by averaging the Rutherford cross-section over all possible electron velocities, similar to the Gerjuoy calculation in equation (3), but was less accurate for small velocities $v < v_{nl}$. The effect of using the EVDF in equation (13) is to populate the EVDF tail with a much larger fraction of high-energy electrons with $v_e \gg v_{nl}$, which gives $f^{\mathrm{Gryz}}(v_e) \sim v_e^{-3}$ instead of $f(v_e) \sim v_e^{-6}$ for the correct EVDF in equation (9). As a result, the average electron kinetic energy $\langle m_e v_e^2/2\rangle$ diverges, which leads to a considerable enhancement of the ionization cross-section at high projectile velocities. For $v \gg v_{nl}$, Gerjuoy's calculation of the differential cross-section $\mathrm{d}\sigma/\mathrm{d}\Delta E(v_e, v, \Delta E)$ of energy transfer ΔE is similar to Gryzinski's. Therefore, we can substitute equation (13) into equations (5) and (4). Because in the limit $v \gg v_{nl}$ the ionization cross-section is proportional to the average electron kinetic energy $\langle m_e v_e^2/2\rangle$ (equation (6)), and the average kinetic energy diverges, it follows that a small population of high-speed electrons contributes considerably to the cross-section. Using the general expression for $\mathrm{d}\sigma/\mathrm{d}\Delta E(v_e, v, \Delta E)$ avoids singularity and yields the logarithmic term in the ionization cross-section similar to the Bethe formula in equation (12). After a number of additional simplifications and assumptions, Gryzinski suggested an approximation for the cross-section in the form given by equation (11) with [21]

$$\sigma^{\mathrm{Gryz}}(v, I_{nl}, Z_p) = \pi a_0^2 Z_p^2 \frac{E_0^2}{I_{nl}^2} G^{\mathrm{Gryz}}\left(\frac{v}{v_{nl}}\right). \tag{14}$$

Here, the function $G^{\mathrm{Gryz}}(x)$ is specified by equation (70) of Formulary. In equation (14), the function $G^{\mathrm{Gryz}}(x)$ has the following limit

$$G^{\mathrm{Gryz}}(x) \to [1 + 0.667\ln(2.7 + x)]/x^2 \quad \text{as } x \to \infty, \tag{15}$$

which is close to Bethe's result in equation (12),

$$G^{\mathrm{Bethe}}(x) \to [1.261 + 0.566\ln(x)]/x^2 \quad \text{as } x \to \infty. \tag{16}$$

For $10 < x < 40$, it follows that

$$G^{\mathrm{Gryz}}(x)/G^{\mathrm{Bethe}}(x) \simeq 1.04. \tag{17}$$

Therefore, the Gryzinski formula can be viewed as a fit to the Bethe formula at large velocities $v \gg v_{nl}$ with some rather arbitrary continuation to small velocities $v \ll v_{nl}$.

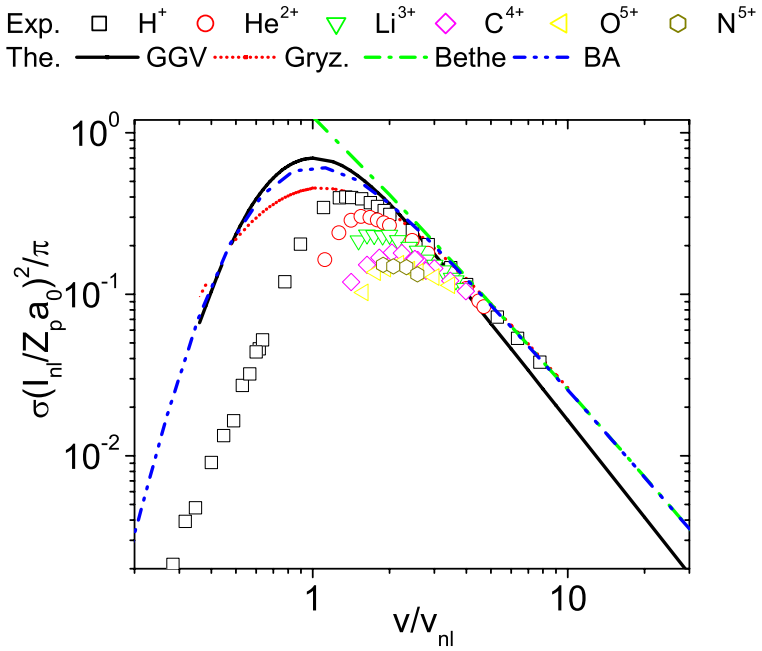

Figure 1. Ionization cross-sections of hydrogen by fully stripped ions showing both experimental data and theoretical fits. GGV stands for the classical calculation in equation (11) due to Gerjuoy using the fit of Garcia and Vriens. Gryz denotes the Gryzinski approximation in equation (14). Bethe stands for Bethe's quantum-mechanical calculation in the Born approximation, limited to $v > v_{nl}$ in equation (12). Finally, BA denotes the Born approximation in the general case in equation (22). All values are in atomic units. For hydrogen, the ionization potential is $I_{nl} = 1/2E_0$, $v_{nl} = v_0 = 2.19 \times 10^8\,\mathrm{cm\,s^{-1}}$, and the cross-section is normalized to $\pi a_0^2/I_{nl}^2 = 3.51 \times 10^{-16}\,\mathrm{cm^2}$. Symbols show experimental data.

2.1.5. Experimental verification of approximate formulae. Figure 1 shows the experimental data for the cross-section for ionizing collisions of fully stripped ions colliding with a hydrogen atom,

$$\mathrm{X}^{q+} + \mathrm{H(1s)} \rightarrow \mathrm{X}^{q+} + \mathrm{H}^{+} + \mathrm{e}, \tag{18}$$

where X^{q+} denotes fully stripped ions of H, He, Li atoms, and (1s) symbolizes the ground state of a hydrogen atom. The experimental data for H^+ ions were taken from [42, 43] (note that authors of this reference concluded that the previous measurements of the cross-sections were inaccurate); from [44] for He^{2+}; and from [45] for Li^{3+} ions. These data were compared to theoretical approximate formulae in [24]. In addition to fully stripped ions, multiple charged ions C^{4+}, N^{5+} and O^{5+} were added from [46]. For these highly charged ions the ionization occurs at large impact parameters, large compared with the electron orbit radius of ions; at these large impact parameters, the force acting on target electron is described by the Coulomb potential, therefore analytical formulae based on the Rutherford scattering should be valid.

From figure 1 it is evident that the Bethe formula describes well the cross-sections for projectile velocities larger than the orbital velocities $v \gg v_{nl}$. At large energies, the GGV formula underestimates the cross-sections as discussed before, whereas Gryzinski's formula gives results

close to the Bethe formula and the experimental data. Both the GGV and Gryzinski formulae disagree with the experimental data at small energies.

2.2. *Behaviour of cross-sections at small projectile velocities* $v \lesssim v_{nl}$

The Bethe, GGV and Gryzinski's formulae fail at small velocities because they assume free electrons, neglecting the influence of the target atom potential on the electron motion during the collision. Apparently the assumption of free electron motion fails if the circulation period of the electron around the atom's nucleus is comparable with the interaction time of an ion with the electron [30]. Let us now estimate the projectile velocities at which the electron circulation needs to be taken into account. The typical impact parameter leading to ionization is

$$\rho_{\text{ioniz}} \simeq \sqrt{\frac{\sigma^{\text{Bohr}}}{\pi}} = \frac{2a_0 v_0^2 Z_p}{v v_{nl}}, \tag{19}$$

and the interaction time is of the order ρ_{ioniz}/v. The electron circulation time is $\tau_{nl} \simeq a_{nl}/v_{nl}$, where v_{nl} is the electron orbital velocity, which scales as $v_{nl} = Z_T v_0$, and a_{nl} is the ion radius $a_{nl} = a_0/Z_T$ [41]. Therefore the condition $\tau_{nl} > \rho_{\text{ioniz}}/v$ holds for $v > v_{\max}$, where

$$v_{\max} = v_{nl}\sqrt{2Z_p/Z_T}. \tag{20}$$

Here, Z_p is the charge of the fully stripped projectile and Z_T is the nuclear charge of the target atom or ion for one electron ions. For general atoms Z_T can be estimated from the ionization potential as $Z_T \approx \sqrt{2I_{nl}/E_0}$. For velocities larger than $v_{\max}$, the ionization cross-section decreases as the velocity increases (see equation (12)) due to the decreasing interaction time with an increase in velocity. On the other hand, for velocities less than $v_{\max}$, the collision becomes more adiabatic. The influence of the projectile is averaged out due to the slower motion of the projectile compared with the electron orbital velocity, and the ionization cross-section decreases with decreasing projectile velocity. Thus, the cross-section has a maximum at $v \simeq v_{\max}$ (equation (20)).

Note that if the projectile speed is comparable with or smaller than the electron orbital velocity $v < v_{nl}$, the Born approximation of quantum-mechanical theory is not valid. Cumbersome quantum-mechanical simulations are necessary for an exact calculation of the cross-sections, as for example in [48]. Nevertheless for the case $2Z_p \sim Z_T$ the maximum of the cross-section calculated from the Born approximation is similar to the experimental results. To describe the behaviour of the cross-section near the maximum, the second-order correction in the parameter v_{nl}/v has been calculated in [49, 50], yielding the cross-section in the form

$$\sigma_{\text{mod}}^{\text{Bethe}}(\tilde{v}) = \pi a_0^2 \frac{E_0^2}{I_{nl}^2}\frac{Z_p^2}{\tilde{v}^2}\left[0.566\,\ln\left(\tilde{v}\right) + 1.26 - 0.66\frac{1}{\tilde{v}^2}\right], \tag{21}$$

where $\tilde{v} = v/v_{nl}$. Equation (21) agrees with the exact calculation in the Born approximation (equation (B.1)) as described in appendix B (the agreement is within 10% for $\tilde{v} > 1.1$). We have developed the following fit for the cross-section in the Born approximation in the general case,

$$\sigma_{\text{fit}}^{\text{BA}}(\tilde{v}) = \pi a_0^2 \frac{E_0^2}{I_{nl}^2}\frac{Z_p^2}{\tilde{v}^2}\left[0.283\ln\left(\tilde{v}^2+1\right) + 1.26\right]\exp\left[-\frac{1.95}{\tilde{v}(1+1.2\tilde{v}^2)}\right]. \tag{22}$$

Equation (22) agrees with the exact calculation (equation (B.1)) within 2% for $\tilde{v} > 1$, and within 20% for $0.2 < \tilde{v} < 1$.

Equations (21) and (22) were derived in the plane wave approximation, i.e., using the unperturbed atomic electron wavefunctions for calculation of matrix elements. This implicitly assumes that the projectile particle transfers momentum to the electron to be ionized quickly at large distances. The electron wavefunction of ionized electron can therefore be described as a continuous spectrum of the target atomic electron, not affected by the projectile.

This assumption breaks down at low projectile velocities when the projectile velocity is comparable with the electron orbital velocity. Indeed, the electron kinetic energy in the frame of the projectile is of order $m_e v^2/2$ and the potential energy $Z_p e^2/\rho_{\text{ioniz}}$, where ρ_{ioniz} is the impact parameter leading to ionization, given by equation (19). Substituting ρ_{ioniz} from equation (19) into electron potential energy $Z_p e^2/\rho_{\text{ioniz}}$ gives that potential energy is larger than kinetic energy if

$$v < v_{nl}. \tag{23}$$

Therefore, under the condition in equation (23), an electron can be effectively captured by the projectile after the collision instead of leading to ionization. As a result, the ionization cross-section is small compared with the charge exchange cross-section at low projectile velocities. The assumption of the unperturbed electron wavefunction results in grossly overestimated ionization cross-sections as can be seen in figure 1.

The ionization cross-sections are also difficult to measure at small projectile energies, because careful separation between the large charge exchange cross-section and the small ionization cross-section is necessary for the correct measurement [42]. Therefore, early measurements of the ionization cross-section at small velocities were not always accurate [16, 42].

2.2.1. Knudsen's treatment. Knudsen modified the Bohr result for ionization to the following form, as discussed, for example, in [47]

$$\sigma^{\text{Knud}}(v) = 2\pi a_0^2 \frac{v_0^2}{v^2} \frac{Z_p^2 E_0}{I_{nl}} \Pi,$$

where

$$\Pi = \left\lfloor \left\lfloor \frac{Z_p v_0 v_{nl}}{v^2} \right\rfloor^{-1} + 2\delta_s \ln \left\lfloor \frac{2v}{v_{nl}} \left\lfloor \frac{2Z_p v_0}{v} \right\rfloor^{-2} \right\rfloor - \left(\frac{2v}{v_{nl}}\right)^{-2} + 1 \right\rfloor - 1. \tag{24}$$

Here, the brackets $\lfloor \ldots \rfloor$ denote the function

$$\lfloor x \rfloor = \begin{cases} x, & \text{for } x > 1, \\ 1 & \text{for } x \leqslant 1. \end{cases}$$

Equation (24) was compared with experimental data in [46], where it was shown that equation (24) overestimates the cross-section for $v > v_{nl}$, and gives even larger disagreement

with the experimental results for $v < v_{nl}$. Another approach, proposed by Gillespie, yielded a good fit to the experimental data.

2.2.2. Gillespie's treatment. To account for the difference between the Born approximation results and the experimental data for $v < v_{\max}$, Gillespie proposed to fit the cross-sections to the following function [23],

$$\sigma^{\text{Gill}}(v) = \exp\left[-\lambda_{nl}\left(\frac{v_0\sqrt{Z_p}}{v}\right)^2\right]\sigma^{\text{Bethe}}_{\text{mod}}(v). \tag{25}$$

Here, λ_{nl} is a constant, which characterizes the ionized atom or ion (for example, for the ground state of H, $\lambda_{nl} = 0.76$), and $\sigma^{\text{Bethe}}_{\text{mod}}$ is the cross-section in the Born approximation in the form of equation (21). Gillespie's equation (25) proved to fit very well existing experimental cross-sections for hydrogen atom ionization by H^+, He^{+2}, Li^{2+}, Li^{3+}, C^{4+}, N^{5+}, N^{+4}, O^{5+} ions, and less well for He and H molecules with the same ions [23, 46]. Because $\sigma^{\text{Bethe}}_{\text{mod}}(v)$ becomes negative for $v < 0.7$, Gillespie's equation (25) cannot be applied to these low projectile velocities. In principle, the general fit $\sigma^{\text{BA}}_{\text{fit}}$ in equation (22) can be used instead of $\sigma^{\text{Bethe}}_{\text{mod}}$ in equation (21). However, because the two formulae differ about 20% in the range of interest, $0.7 < v < 1$, the fitting coefficients λ_{nl} may have to be updated for better fit for use with $\sigma^{\text{BA}}_{\text{fit}}$.

Although Gillespie's fit proved to be very useful, there are a number of reasons to look for another fit, mostly because fitting coefficients λ_{nl} are not known prior measurements for any target atoms. For example, Gryzinski's equation (14) is frequently used, because it requires only knowledge of one function for calculations of cross-sections, notwithstanding the fact that it overestimates the cross-sections at low energies.

2.2.3. v^2/z_p scaling. For $v \lesssim v_{nl}$, a universal curve is expected if both the cross-sections and the square of impact velocity are divided by Z_p [53]. This scaling was established for the total electron loss cross-section σ^{el}, which includes both the charge exchange cross-section σ^{ce} and the ionization cross-section. Based on the results of CTMC calculations, Olson proposed the following fit [54],

$$\sigma^{\text{el}}(v, Z_p) = Z_p A_{nl}\pi a_0^2 f^{\text{Olson}}\left(\frac{v}{v_0\gamma_{nl}\sqrt{Z_p}}\right), \tag{26}$$

where $f(x)$ describes the scaled cross-sections

$$f^{\text{Olson}}(x) = \frac{1}{x^2}[1 - \exp(-x^2)]. \tag{27}$$

Here, γ_{nl} and A_{nl} are constants, for example, $\gamma_{\text{H}} = \sqrt{5/4} = 1.12$ and $A_{\text{H}} = 16/3$ for atomic hydrogen, and $\gamma_{\text{He}} = 1.44$ and $A_{\text{He}} = 3.57$ for helium. The scaling in equation (26) was also demonstrated analytically by Janev [56]. For $v \ll v_0\sqrt{Z_p}$, σ^{el} is dominated by charge exchange, $\sigma^{\text{ce}} \approx \sigma^{\text{el}}$, and equation (26) gives a constant cross-section for charge exchange, $\sigma^{\text{ce}} \approx \sigma^{\text{el}} = 16\pi Z_p/3a_0^2$. For $v \gg v_0\sqrt{Z_p}$, σ^{el} is dominated by the ionization cross-section, and $\sigma^{\text{ce}} \approx \sigma^{\text{high-energy}}_{\text{classical}}$ (equation (6)). Note that the scaling in equation (26) does not reproduce the

logarithmic term in the Bethe formula (equation (12)) for $v \gg v_0\sqrt{Z_p}$ because it is based on classical trajectory calculations. To make equation (26) agree with equation (6), the coefficients γ_{nl} should be proportional to $\sqrt{I_{nl}}$. For example, the ionization potential for hydrogen is $I_{\rm H} = 13.6\,{\rm eV}$, and for helium $I_{\rm He} = 24.6\,{\rm eV}$. The ratio of $\gamma_{\rm H} = 1.12$ to $\gamma_{\rm He} = 1.44$ differs from $\sqrt{I_{\rm H}}/\sqrt{I_{\rm He}}$ by only 5%, i.e., $\gamma_{\rm H}/\sqrt{I_{\rm H}}/(\gamma_{\rm He}/\sqrt{I_{\rm He}}) = 1.05$. Therefore, as was shown by Janev [56], the scaling in equation (26) can be rewritten in a form similar to equation (11) by normalizing the velocity to v_{nl}, equation (10), i.e.,

$$\sigma^{\rm el}(v, I_{nl}, Z_p) = \pi a_0^2 Z_p N_{nl} \frac{E_0^2}{I_{nl}^2} B_{nl} G^{\rm el}\left(\frac{v}{v_{nl}\sqrt{Z_p}}\right), \tag{28}$$

where

$$G^{\rm el}(x) = \tfrac{4}{3} f^{\rm Olson}(x/\gamma_{\rm H}). \tag{29}$$

Here, N_{nl} is the number of electrons in the orbital nl, and the B_{nl} factors equation (7) are introduced to account for the difference of the orbital EVDFs with the hydrogen-like EVDF function in equation (9). By construction, equation (28) coincides with equation (6) in the limit $v \gg v_{nl}\sqrt{Z_p}$.

Because the scaling in equation (26) is based on classical trajectory calculations, it is valid only for intermediate velocities where the underbarrier transitions allowed in the quantum-mechanical calculations do not contribute significantly (see appendix B for details). Experimental data [45, 56] confirm the scaling in equation (26) for $1.2 < v/(v_{nl}\sqrt{Z_p}) < 3$, or equivalently, for the projectile energy in the range $E = 30$–$200 \times Z_p I_{nl}/I_{\rm H}$ in units of keV amu^{-1}.

A similar scaling to equation (26) was derived in [80] based on quantum-mechanical calculations making use of the quasi-classical approach developed originally by Keldysh for multi-photon ionization of atoms in a strong electromagnetic field. These calculations give scaling similar to equation (26), but with a different function $f(x)$ given in [80]. The quantum-mechanical calculation results for the charge exchange cross-section in [80] are a factor of 3 larger than Olson's cross-section in equation (26) for $v/(v_0\sqrt{Z_p}) < 0.2$. Experimental data presented in [44] show that equation (28) underestimates the charge exchange cross-section in the velocity range $0.2 < v/(v_0\sqrt{Z_p}) < 0.5$ by about 40%, see figure 2. To mitigate the discrepancy, the authors of [55] modified the representation of the electron energy distribution function: instead of making use of the classical microcanonical ensemble with a single value of the total electron energy corresponding to the binding energy, they used several values of binding energy for a better representation of the radial electron distribution functions by adding a spread in the binding energy. This resulted in enhanced cross-section values (by about 40%) and better matching with the experimental data. However, the additional tunnelling effect, not accounted for in the classically trajectory method, can be important for very small velocities [80] and leads to a logarithmic dependence of the cross-sections at low ion velocities $v/(v_0\sqrt{Z_p}) \ll 0.2$, as seen in experimental data [19], see figure 2.

Direct application of the scaling in equation (28) for the ionization cross-section instead of the total electron removal cross-section does not produce a single scaled function (see figure 3 for hydrogen and figure 5.(b) for helium). Furthermore, the data are considerably scattered near the maxima of the cross-sections.

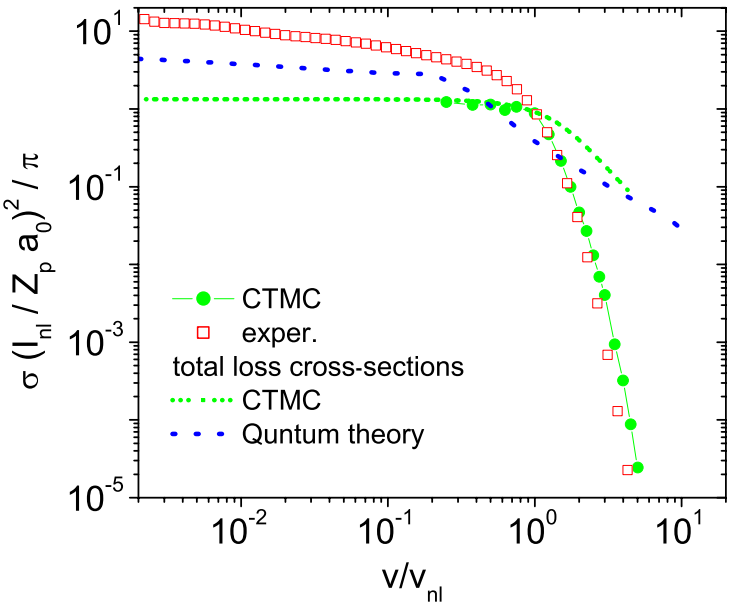

Figure 2. Electron capture and total electron loss cross-sections of hydrogen by protons showing both the experimental data presented in [44] and the theoretical fits. CTMC calculations are shown together with the fit formula for CTMC calculations equation (28) and quantum-mechanical calculation of [80].

2.2.4. Adiabatic scaling. In the region of projectile velocities $v \ll v_{nl}$, several authors developed adiabatic theories of electron ionization [83, 84, 86, 87]. If the projectile velocity is small compared with the orbital velocity, the collision is adiabatic and the electron circulates many times near both nuclei. The electronic energy states need to be determined in such a 'quasi-molecule' as a function of the internuclear distance R. The ionization is determined from the singularities of the energy surfaces as a function of distance between the nuclei. It has been shown that these nonadiabatic regions are associated with the branching points of the adiabatic potential energy of the system, analytically continued in the complex R plane, the so-called 'hidden crossing'. Based on this theory, a scaling for the cross-section was proposed in [87]

$$\sigma(v, Z_p) = Z_p A\pi a_0^2 \frac{v}{v_{nl}} f_z(Z_p) \exp\left[-\frac{c v_{nl}}{v f_z(Z_p)}\right], \tag{30}$$

where $f_z(Z_p) = (1+\lambda)/(1+\lambda Z_p^{1/4})$, and A, c and λ are constants. For example, for hydrogen ionization, $A = 0.96$, $c = 1.71$ and $\lambda = 0.275$. The scaling was verified experimentally for H^+–H collisions for $0.2 < v < 0.5$ in [43], and additional details are given in section 3. In [64, 65], it was shown that the experimental data for the ionization of hydrogen and helium can be described by the scaling law in the range $0.6 < v/v_{nl}Z_p^{1/4} < 1.5$ for $Z_p \gg 1$

$$\sigma(v, Z_p)/Z_p = A\pi a_0^2 \left(\frac{v}{v_{nl} Z_p^{1/4}}\right) \exp\left[-\frac{c v_{nl} Z_p^{1/4}}{v}\right], \tag{31}$$

where $v_{nl} = \sqrt{2I_{nl}/E_0}$, $A = 115$ and $c = 7.9$ for helium.

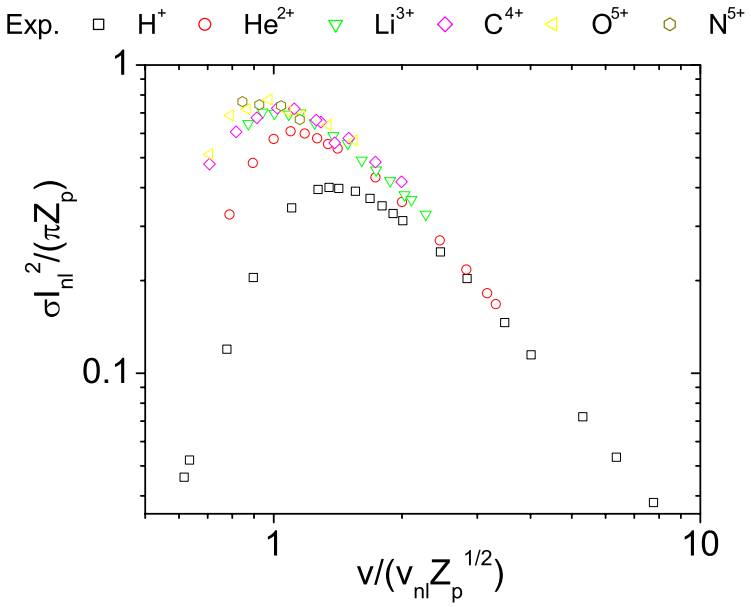

Figure 3. Ionization cross-sections of hydrogen by fully stripped ions. The scaled experimental data are from figure 1. Note that the data do not merge into a single curve.

2.3. Scaling of ionization cross-sections over a wide velocity range

To describe the ionization cross-sections over a wide velocity range it is necessary to predict the location of the cross-section maximum as a function of projectile velocity. This was performed in [89].

2.3.1. Saddle-point scaling for cross-section maximum. If the value of projectile velocity is in the region near the maximum of the cross-section, the classical mechanical description should yield an accurate result. In this range of velocities $v/v_{nl}Z_p^{1/2} \approx 1.5$, see figure 3, the collision time is comparable with the electron circulation time, and an ejected electron in the ionizing collisions moves in the combined field of the nuclei. Because this electron is attracted by both the projectile and target nuclei, the 'easiest' way to escape from the nuclei corresponds to electron ejection into a region where the attracting forces cancel each other, i.e., near the saddle point (although not exactly at the saddle point). The saddle point moves with velocity [82]

$$v_{\mathrm{sp}} = \frac{v}{1+\sqrt{Z_p/Z_T}}. \tag{32}$$

Therefore the maximum of the cross-section should correspond to conditions where $v_{\mathrm{sp}} \simeq a v_{nl}$, where a is a coefficient of order unity. Substituting this condition into equation (32) gives for the

position of the cross-section maximum [89]

$$v_{\max} = a v_{nl}\left(1 + \sqrt{Z_p/Z_T}\right). \tag{33}$$

A fit of the experimental data gives $a = 0.7$ for the ionization of hydrogen [89]. To eliminate the numerical coefficient, another scaling was proposed for neutral targets with $Z_T \sim 1$ in [24]

$$v_{\max} = v_{nl}\sqrt{1 + Z_p}. \tag{34}$$

Equations (33) and (34) give similar estimates (within 10% for $Z_T = 1$ and $Z_p \leqslant 7$).

2.4. Fit formula for the ionization cross-section in wide velocity range

Analysis of the experimental data in figure 1 shows that the maxima of the experimentally measured cross-sections occur at $\sqrt{Z_p/Z_T + 1}$, not at $\sqrt{Z_p/Z_T}$ as would be the case according to scaling in equation (28). Therefore, it is natural to plot cross-sections as a function of the normalized velocity $v/(v_{nl}\sqrt{Z_p/Z_T + 1})$. Note that at large velocities, according to equation (6) $\sigma \sim Z_p^2/v^2$. Therefore, making use of the normalized velocity $v/(v_{nl}\sqrt{Z_p/Z_T + 1})$ requires normalization of the cross-sections according to $\sigma/[Z_p^2/(Z_p/Z_T + 1)]$. As a consequence, instead of equation (28), the following scaling was proposed in [24]

$$\sigma^{\text{ion}}(v, I_{nl}, Z_p) = \pi a_0^2 \frac{Z_p^2}{(Z_p/Z_T + 1)} N_{nl} \frac{E_0^2}{I_{nl}^2} G^{\text{new}}\left(\frac{v}{v_{nl}\sqrt{Z_p/Z_T + 1}}\right). \tag{35}$$

Resulting plots of the scaled cross-sections are shown in figure 4. Comparing figures 3 and 4 one can clearly see that all of the experimental data merge close to each other on the scaled plot based on equation (35).

The resulting universal function can be fitted with various functions, but the simplest fit was proposed by Rost and Pattard [58]. They showed that if both the cross-section and the projectile velocity are normalized to the values of cross-section and projectile velocity at the cross-section maximum, then the scaled cross-section $\sigma/\sigma_{\max}$ is well described by the fitting function

$$\sigma(v) = \sigma_{\max} \frac{\exp(-v_{\max}^2/v^2 + 1)}{v^2/v_{\max}^2}. \tag{36}$$

Here, $\sigma_{\max}$ is the maximum of the cross-section, which occurs at velocity $v_{\max}$. For the case of the ionization cross-section by the bare projectile, it was shown in [24] that

$$\sigma_{\max} = \pi a_0^2 B_{nl} \frac{Z_p^2}{(Z_p/Z_T + 1)} \frac{E_0^2}{I_{nl}^2}, \tag{37}$$

$$v_{\max} = v_{nl}\sqrt{Z_p/Z_T + 1}, \tag{38}$$

where the coefficients B_{nl} depend only weakly on the projectile charge. From figure 4 one can estimate $B_{nl} = 0.8$ for the ionization of hydrogen by protons, while for ionization of hydrogen by bare nuclei of helium and lithium, we find $B_{nl} = 0.93$. As can be seen from figure 4, the

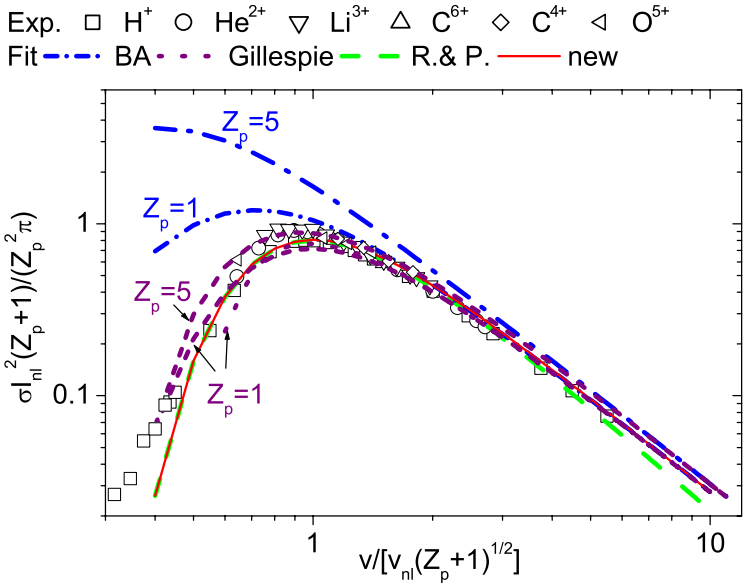

Figure 4. Ionization cross-sections of hydrogen by fully stripped ions showing the scaled experimental data and the theoretical fits. BA denotes the Born approximation (equation (22)) for $Z_p = 1, 5$. 'Gillespie' denotes Gillespie's fit according to equation (25) combined with equation (21) for $Z_p = 1, 5$ and equation (25) combined with $\sigma_{\rm fit}^{\rm BA}$ in equation (22) for $Z_p = 1$. R & P symbolizes the fit proposed by Rost and Pattard [58] in equation (36). 'New' denotes the new fit given by equation (38).

function in equation (36) with $\sigma_{\rm max}$ and $v_{\rm max}$ defined in equation (37) describes well the cross-sections at small and intermediate energies, but underestimates the cross-section at high energies. The reason is that the function in equation (36) does not reproduce the logarithmic term in the Bethe formula in equation (12). To improve the agreement with the experimental data and the Bethe formula we propose a new scaling for the fitting function in equation (35) defined by

$$G^{\rm new}(x) = \frac{\exp(-1/x^2)}{x^2}[1.26 + 0.283\ \ln(2x^2 + 25)]. \tag{39}$$

At large $x \gg 1$, equation (39) approaches the Bethe formula in equation (16), and at small $x < 1$, equation (39) approaches the result in equation (36). The function $G^{\rm new}(x)$ has a maximum at $x \simeq 1$, with $G^{\rm new}(1) \simeq 0.86$. Because 0.86 is in between the maxima of the scaled cross-section of hydrogen by protons ($B_{nl} = 0.8$) and the cross-section for ionization of hydrogen by bare nuclei of helium and lithium ($B_{nl} = 0.93$), we did not incorporate the coefficients B_{nl} in equation (39). This gives it a general form and introduces small errors of less than 8%.

The fit in equation (39) predicts an extremely small cross-section at very low velocity $\sigma_{\rm fit}^{\rm low-energy}(v) \sim \exp[-(Z_p/Z_T + 1)v_{nl}^2/v^2]$, whereas equation (30) gives $\sigma(v) \sim \exp[-cv_{nl}f_z(Z_p)/v]$. Therefore, the numerical fit in equation (39) underestimates the cross-section for $v < 0.5$ (more details are given in section 3).

We have applied the new fit in equations (35) and (39) to the ionization cross-sections of helium and lithium, in addition to hydrogen, assuming $Z_T = 1$ and $v_{nl} = v_0\sqrt{2I_{nl}/E_0}$. The symbols in figure 5(a) denote the experimental data for H^+, He^{+2}, Li^{3+} [59, 60], for C^{6+} and

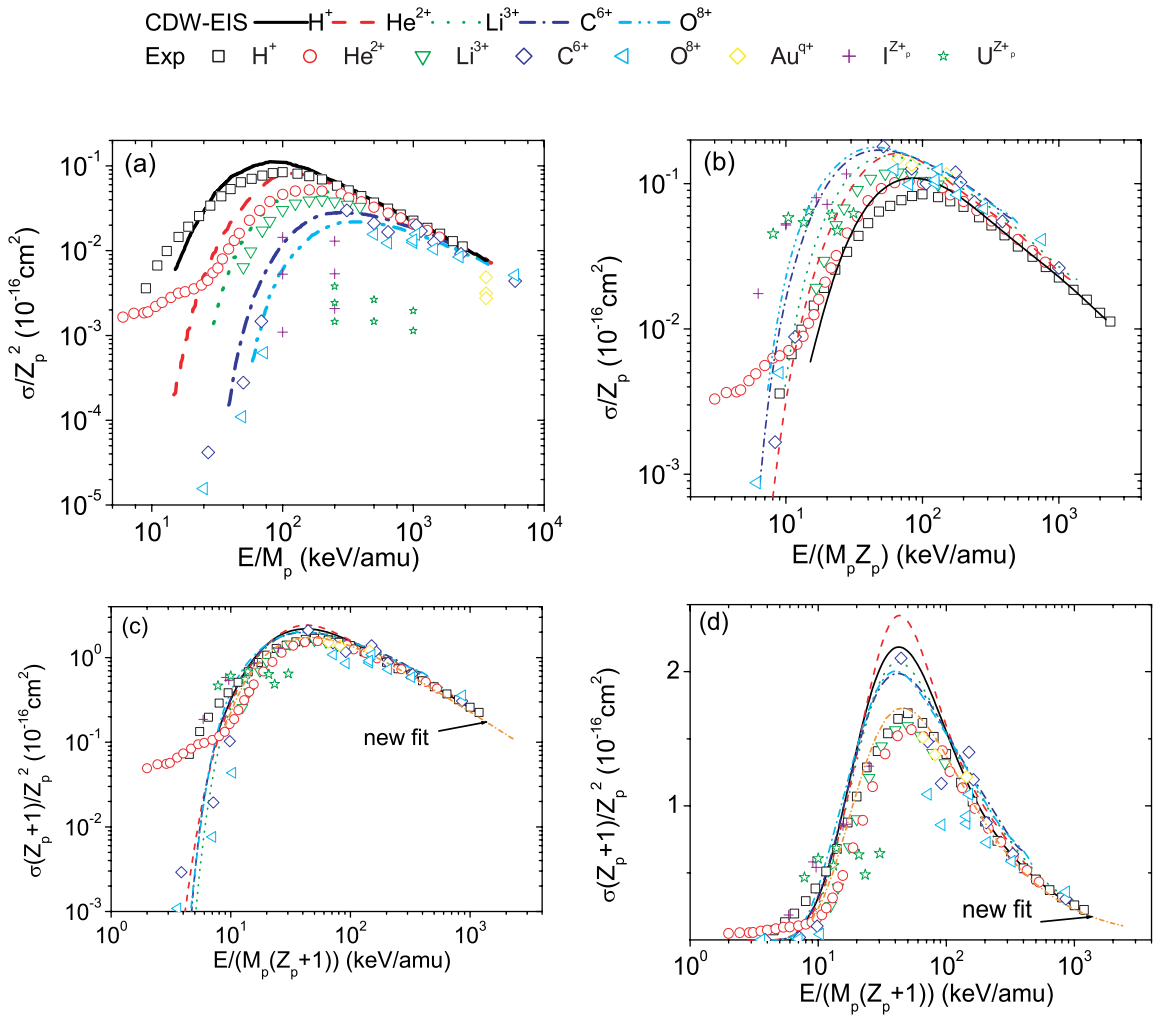

Figure 5. Ionization cross-sections of helium by various stripped ions. The solid curves correspond to the CDW-EIS theoretical calculation, and the symbols label the experimental data (see text for details). Shown in the figures are: (a) the raw data; (b) the scaled data from figure 4(a), making use of equation (28); (c) the scaled data making use of equation (35); and (d) the experimental data scaled using only equation (35) together with the fit function. The notation 'new fit' denotes equation (39).

O^{8+} [47], [61]–[65]. These data were shown in [24]. In addition, we have added to the plot experimental data for I^{Z_p+} and U^{Z_p+} [66], and for Au^{Z_p+} [67], where $Z_p = 10$–40. We have included partially stripped ions with large Z_p, because as shown in [68] the ionization cross-sections near the maximum depends only on projectile charge and is independent of internal structure of the projectile. This is likely because the ionization occurs at impact parameters larger than the radius of the inner structure of the projectile.

The solid curves correspond to the continuum-distorted-wave-eikonal initial state (CDW-EIS) theoretical calculation from [69], which is a generalization of the Born approximation. The CDW-EIS theory accounts for the distortion of the electron wavefunction by the projectile. From figure 5(a) it is evident that the CDW-EIS theory overestimates the cross-section near the maximum, and underestimates the cross-section at small energies. Note also from figure 5(a) the large scatter of the data for C^{6+} and O^{8+} ions, compared with the recommended data in [44] (based on Gillespie's fit) not shown in the plots. This is likely because the data were assembled from many different sources, [47], [61]–[65], and may be attributed to an unsatisfactory absolute calibration of the cross-sections in some of the data.

Direct application of the scaling formula in equation (28) to the ionization of helium does not produce similar good results to the hydrogen case (see figure 5(b)). But after applying the new scaling in equation (35), all of the experimental and theoretical results merge close together on the scaled plot, as is clearly evident in figure 5(c). Moreover, if we use the fit function of velocity normalized to the orbital velocity v_{nl} estimated from the ionization potential of helium ($I_{\mathrm{He}} = 24.6\,\mathrm{eV}$) making use of equation (10), the cross-section is given by the same scaling as in equation (35) with the same function as in equation (39), as evident from figure 5(d). (The number of electrons in the helium atom is $N_{nl} = 2$, and therefore the scaled cross-section is twice that of hydrogen.) From figure 5(d) it is clear that the new proposed fit in equation (35) using the function in equation (39) gives very good results for both hydrogen and helium. The discrepancy between the new fit and the helium data at very small velocities is discussed in the next section.

Note that one experimental point in figure 5 for C^{6+} projectiles is located far away from the fit. The error bar for this point is about 30% [61]. These data may be inaccurate, as the experimental point is higher than the predictions of CDW-EIS theory, which overestimates the cross-section near the maxima of the cross-sections for all other ions. The reason for the large scatter in the uranium data on the scaled plot at small energies is not clear, because the experimental data for all other projectiles are located much closer to the fit line. This may be due to the contribution of autoionization when the projectile velocity is low [68]. The other reason is that the ionization cross-section is larger (about $10^{-15}\,\mathrm{cm}^{-2}$) than the helium atom size. Therefore, two electrons are most likely to be removed during the collisions, and simple one-electron scaling must be corrected by the larger effective ionization potential needed to remove two electrons simultaneously. (The uranium ions had energies and charges: 250 keV, $Z_{\mathrm{p}} = 17, 24, 31$; 500 keV, $Z_{\mathrm{p}} = 23, 27$; and 1 MeV, $Z_{\mathrm{p}} = 32, 42$ respectively.)

We have also performed a comparison of the scaling with available experimental data for the ionization of the lithium atoms [70, 71], as shown in figure 6. From figure 6, it is evident that the fit describes the cross-section well, except for values of the cross-section near the maximum. It is surprising that the Bethe formula in equation (12) describes the cross-sections well up to the maximum. The calculation in [72] also leads to much smaller values than the experimental data. Reference [71] quotes 50% uncertainty in the experimental data, whereas [70] claims only 10% uncertainty.

Further verification of the scaling is difficult because reliable experimental data and numerical simulations for a broad range of projectile velocities are absent for other atoms.

A number of other semi-empirical models have been developed for the ejected electron velocity distributions. They typically use up to ten fitting parameters to describe the differential ionization cross-sections as a function of ejected electron velocity, projectile velocity and charge [19].

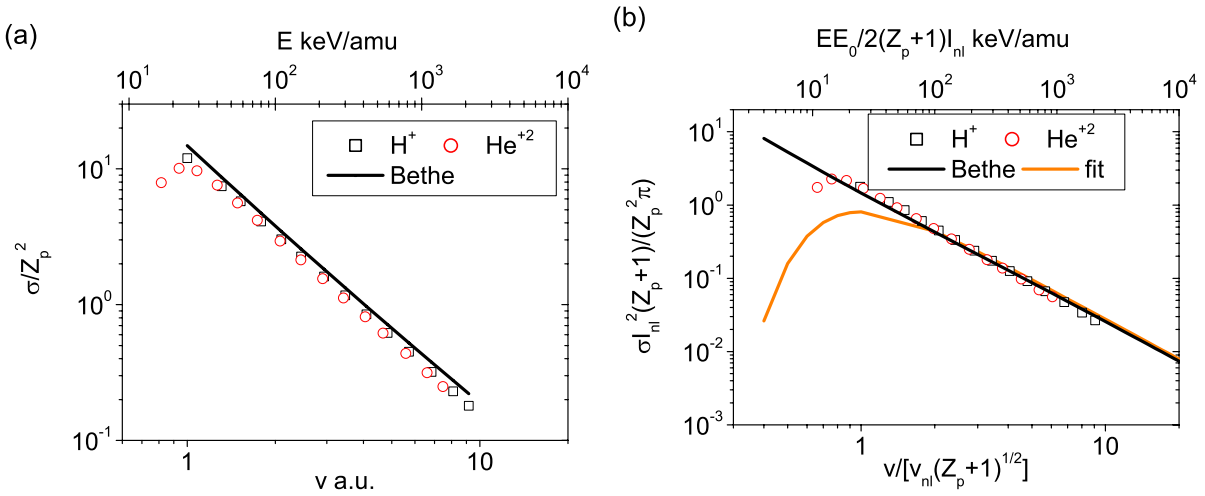

Figure 6. Ionization cross-sections of lithium by H^+ and He^{+2}. The symbols show experimental data (see text for details). Shown in the figures are: (a) the raw data and the Bethe formula, equation (12); (b) the scaled data making use of equation (35) together with the fit function. The notation 'new fit' denotes equation (39).

Scaling laws for single and multiple electron loss from projectiles in collisions with a many electron target were proposed in [27, 90].

3. Brief survey of theoretical approaches and their limitations for ionization cross-section

In this section, we present a brief survey of the theoretical approaches to cross-section calculations and their limitations. Theoretical justifications are also given for the fit formulae in equations (35) and (39). We begin with an analysis for high projectile velocities.

3.1. Behaviour of cross-sections at large projectile velocities $v > v_{nl}$

At high projectile velocity $v \gg v_{nl}$, the Born approximation can be applied for the cross-section calculation. The applicability of the Born theory and the Bethe formula in equation (12) was studied by comparison with available experimental data in [34, 61, 67], [73]–[75]. It was confirmed that the necessary condition for the validity of the Bethe formula is given by [29, 30]

$$v > \max(2Z_p v_0, v_{nl}). \tag{40}$$

The first condition in equation (40) assures that the projectile potential is taken into account in the Born approximation; the second condition allows use of the unperturbed atomic wavefunction.

The failure of the Bethe formula for large Z_p is apparent from the experimental data for gold ions shown in figure 5(a). The ion velocity corresponds to $v = 12v_0$ or $v = 8.9v_{nl}$, whereas $Z_p = 24, 43$ and 54, and does not satisfy the condition in equation (40). As a result, the cross-sections are much smaller than given by the Bethe formula, as evident from figure 5(a). At large projectile energies, all data merge to the Bethe formula, which corresponds to a straight line in

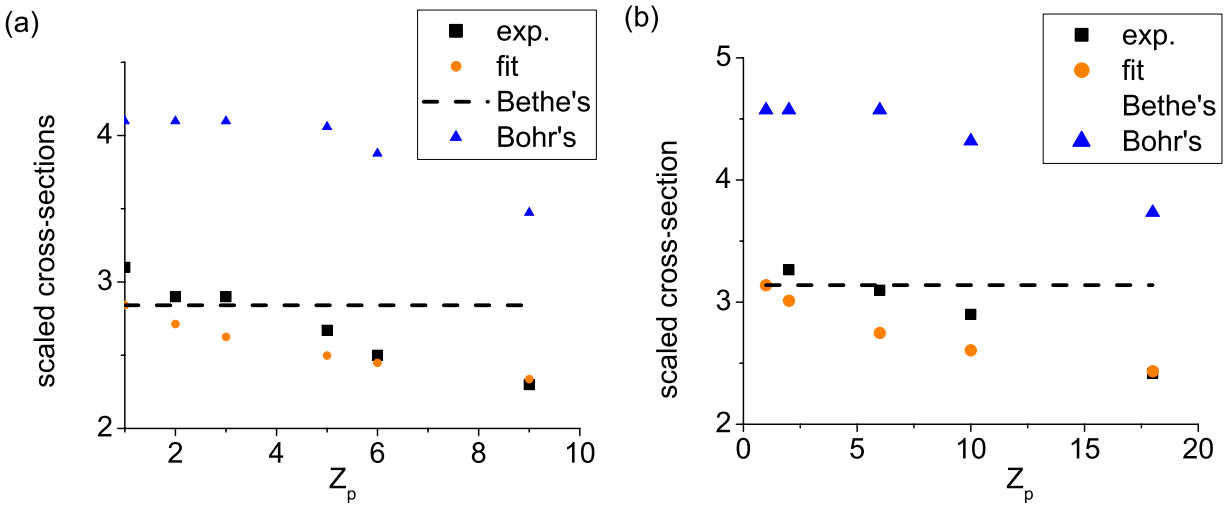

Figure 7. Scaled ionization cross-sections ($\sigma v^2/4\pi a_0^2 Z_p^2 v_0^2$) of helium by fast fully stripped ions as a function of charge for ion energies (a) 2.31 MeV amu^{-1}, and experimental data from [73]; and (b) 6 MeV experimental data from [34]. Shown in the figures are the raw data, the calculation making use of the Bethe formula (equation (12)), the Bohr formula (equation (24)), and the theoretical fit (equation (35)).

a logarithmic plot, similar to figure 1. For uranium and iodine data, the velocity is few times the electron orbital velocity, but the charge for uranium varies from 17 to 42, and for iodine from 5 to 25. As a result, the condition in equation (40) is not satisfied, and the cross-section is considerably smaller than predicted by the Bethe formula.

In the region of high projectile velocities the new fit predicts the ionization cross-section

$$\sigma_{\text{fit}}^{\text{high-energy}}(v) = 4\pi a_0^2 \frac{v_0^4}{v_{nl}^2} \frac{Z_p^2}{v^2} \left[0.566 \ln \left(\frac{v}{v_{nl}\sqrt{(Z_p+1)/2}} \right) + 1.26 \right], \tag{41}$$

which differs from the Bethe formula in equation (12). (The factor $\sqrt{(Z_p+1)/2}$ appears in the denominator under the logarithm in the first term on the right-hand side of equation (41).) We claim that incorporating this factor gives a better cross-section estimate than the Bethe formula. The authors of [34, 61, 67, 73] have studied the ionization cross-section at a given velocity as a function of charge state. The comparison of the experimental data with the Bohr formula was performed in [73] for the ionization of helium by fast ions with charge varying from one to six at ion energies of 0.64, 1.44 and 2.31 MeV. A comparison of the experimental data from [34, 73] with the Bethe (equation (12)), Bohr (equation (24)), and fit (equation (35)) formulae is shown in figure 7.

From figure 7 it is evident that equation (35) describes the experimental data within an experimental uncertainty of about 8% [34].

A comparison of the experimental data for ionization of hydrogen from figure 1 with the Bethe formula in equation (12) and the fit formula in equation (41) is shown in figure 8. The experimentally estimated uncertainty of 5.5% [45] is shown by the error bar. Figure 8 shows

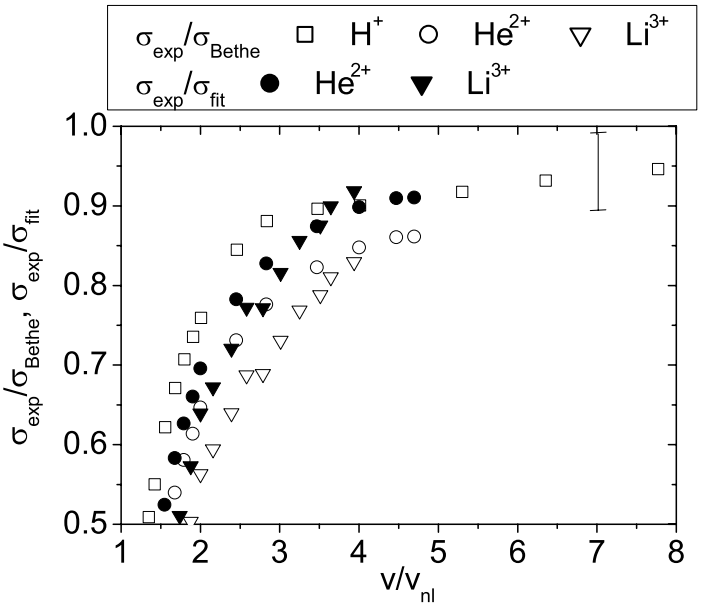

Figure 8. Ratio of ionization cross-sections of hydrogen by fully stripped ions to the Bethe formula in equation (12) and the fit formula in equation (41) at high velocities. The experimentally estimated uncertainty of 5.5% [45] is shown by the error bar.

that the Bethe formula describes the experimental data for ionization of hydrogen by protons within the error bar only for $v > 6v_0$. Application of the fit formula instead of the Bethe formula reduces discrepancy with the data.

The applicability of the Bethe formula is limited by the validity of the Born approximation. One of the easiest ways to correct it was suggested in [80]. Firstly, the Born approximation is considered, making use of a classical trajectory for the projectile and a quantum-mechanical description in the Born approximation for the electron. In this approximation, the probability of ionization or excitation is a function of the impact parameter ρ. Here, for brevity, we shall consider only ionization of the hydrogen atom. The projectile particle interacts with the atomic electron with a potential energy $V(\mathbf{R}, \mathbf{r}_e) = -Z_p e^2/|\mathbf{R} - \mathbf{r}_e|$, where $\mathbf{R}(t) = \rho + \mathbf{v}t$ is the classical trajectory of the projectile particle, and $\mathbf{r}_e$ describes the position of the electron relative to the nucleus of the atom. For any impact parameter ρ, the probability of ionization is given by the square of the transition amplitude

$$P_{\mathrm{BA}}(\rho) = \frac{1}{\hbar^2}\left|\int \mathrm{d}\mathbf{r}_e \Psi_i(r_e)\left[\int \mathrm{d}t\ \mathrm{e}^{\mathrm{i}\Delta E t/\hbar} V(\mathbf{R}, \mathbf{r}_e)\right]\Psi_f^*(r_e)\right|^2. \tag{42}$$

Here, ΔE is the transferred energy in the transition, and Ψ_i and Ψ_f are the initial and final electron wavefunctions, respectively. It can be shown that the calculations of ion–atom ionization cross-sections using the conventional Born approximation describing the collision making use of momentum transfer (outlined in appendix B) and the semiclassical Born approximation making use of the assumption of the straight line classical projectile trajectory (equation (42)) are equivalent [41].

For large impact parameters $\rho \gg a_0$, we can expand $V(\mathbf{R}, \mathbf{r}_e)$ in powers of $\mathbf{r}_{enl}/R$ according to

$$V(\mathbf{R}, \mathbf{r}_e) = Z_p e^2 \left(-\frac{1}{R} + \frac{\mathbf{R} \cdot \mathbf{r}_e}{R^3} \right). \tag{43}$$

The first term does not contribute to the matrix element in equation (42) due to the orthogonality of the final and initial states. Substituting equation (43) into equation (42) and integrating in time yields [41]

$$P_{\mathrm{BA}}(\rho) = \left(\frac{2Z_p v_0}{\rho v} \right)^2 \left| \int \mathrm{d}\mathbf{r}_e \; \Psi_i(r_e) \Psi_f^*(r_e) \left[\frac{\omega\rho}{v} x_e K_1 \left(\frac{\omega\rho}{v} \right) + \mathrm{i} z_e \frac{\omega\rho}{v} K_0 \left(\frac{\omega\rho}{v} \right) \right] \right|^2, \tag{44}$$

where $\omega = \Delta E/\hbar$, and K_n is the modified Bessel function. Expanding the Bessel functions for small and large arguments, or simply evaluating the integrand in equation (44) approximately, we can approximate

$$\frac{\omega\rho}{v} K_1 \left(\frac{\omega\rho}{v} \right) = \begin{Bmatrix} 1, & \omega\rho/v < 1 \\ 0, & \omega\rho/v > 1 \end{Bmatrix}, \tag{45}$$

and neglect the second term on the right-hand side in equation (44), which is small compared with the first term. The probability of ionization vanishes for $\rho > \rho_{\max} \simeq v/\omega = 2a_0 v/v_0$, corresponding to the adiabatic limit. For $\rho > \rho_{\max}$, the collision time $\rho_{\max}/v > a_0/v_0$ is much longer than the electron circulation time around the nucleus, and the collision is adiabatic. Consequently, the ionization probability is exponentially small for $\rho > 2a_0 v/v_0$.

The square of electron dipole matrix element averaged over all possible momenta of the ionized electron is [40]

$$\sum_f \int \mathrm{d}\mathbf{r}_e \left| \Psi_i(r_e) x_e \Psi_f^*(r_e) \right|^2 = 0.283 a_{nl}^2. \tag{46}$$

Note that the sum over all final states including *both* ionization and excitation gives

$$\sum_f \langle 0|x_e|f\rangle\langle f|x_e|0\rangle = \langle 0|x_e^2|0\rangle = \tfrac{1}{3}\langle 0|r_e^2|0\rangle = a_{nl}^2. \tag{47}$$

In this sum, 0.717 corresponds to excitation, and 0.283 corresponds to ionization [40].

For large impact parameters the momentum transfer to the electron is small and we can neglect the electron kinetic energy of the ejected electron compared with the ionization potential. As a result, $\Delta E \approx I_{nl}$ and $\omega = v_0 I_{nl}/a_0 E_0 = v_{nl}^2/v_0 a_0$ (in atomic units). Finally for $\rho > a_{nl}$, the ionization probability is

$$P_{\mathrm{BA}}(\rho) \approx 0.283 \left(\frac{2a_{nl} v_0 Z_p}{\rho v} \right)^2 \begin{Bmatrix} 1, & \rho < a_0 v v_0 / v_{nl}^2 \\ 0, & \rho > a_0 v v_0 / v_{nl}^2 \end{Bmatrix}. \tag{48}$$

The ionization cross-section is given by the integral

$$\sigma = 2\pi \int_0^\infty P_{\mathrm{BA}}(\rho) \rho \, \mathrm{d}\rho. \tag{49}$$

For $\rho > a_{nl}$, we can use equation (48) to estimate $P_{\rm BA}(\rho)$. For $\rho < a_{nl}$, the dipole approximation in equation (43) is not valid. To evaluate $P_{\rm BA}(\rho)$ approximately for $\rho < a_0$, we can utilize the fact that $\int {\rm d}t\ {\rm e}^{{\rm i}\Delta Et/\hbar} V(\mathbf{R}, \mathbf{r}_e)$ is a weak function of ρ for $\rho < a_{nl}$, and therefore $P_{\rm BA}(\rho) \approx P_{\rm BA}(a_{nl})$. Substituting $P_{\rm BA}(\rho) \approx P_{\rm BA}(a_{nl})$ for $\rho < a_{nl}$, and $P_{\rm BA}(\rho)$ from equation (48) for $\rho > a_{nl}$, into equation (49) gives

$$\sigma = 8\pi a_{nl}^2 \cdot 0.283 \frac{v_0^2 Z_p^2}{v^2} \left[\tfrac{1}{2} + \ln\left(\frac{a_0 v v_0}{a_{nl} v_{nl}^2} \right) \right]. \tag{50}$$

The first term in equation (50) comes fromcontributions of impact parameters $\rho < a_{nl}$, and the second term originates from contributions of large impact parameters $\rho > a_{nl}$, respectively. Comparison with the exact result in the Born approximation in equation (12) shows that the contribution of impact parameters $\rho < a_{nl}$ is underestimated, and $1/2$ should be replaced by 2.23. *The above considerations are valid if the total probability of ionization and excitation* ($P_{\rm BA}^{\rm tot}(\rho) = (2Z_p a_{nl} v_0/\rho v)^2$, *for* $\rho > a_{nl}$) *for the entire region of impact parameters is less than unity, which requires* $2Z_p v_0/v < 1$. *Hence, the condition for the Born approximation validity equation (40).* (Note that the total probability of ionization and excitation is about four times larger for ionization only.)

For $2Z_p v_0/v > 1$, the total probability of the ionization and excitation $P_{\rm BA}^{\rm tot}(\rho)$ calculated using the Born approximation is more than unity, $P_{\rm BA}^{\rm tot}(\rho) > 1$, for impact parameters $\rho < \rho_{\rm break} = 2Z_p a_0 v_0/v$, indicating the breakdown of the Born approximation [80]. Similar to the previous case, we can estimate the ionization probability $P_{\rm BA}(\rho)$ from equation (48) for $\rho > \rho_{\rm break} > a_0$ and assume $P_{\rm BA}(\rho) \approx P_{\rm BA}(\rho_{\rm break}) = 0.283$ for $\rho < \rho_{\rm break}$. These considerations result in a cross-section estimate similar to the Bethe formula but with the logarithmic term in the form $\ln(\rho_{\max}/\rho_{\min}) = \ln(v^2/v_{nl}^2 2Z_p)$, which gives

$$\sigma = 8\pi a_0^2 \cdot 0.283 \frac{v_0^2 Z_p^2}{v^2} \left[\frac{1}{2} + \ln\left(\frac{v^2}{2v_{nl}^2 Z_p} \right) \right]. \tag{51}$$

This calculation results in a smaller cross-section than the Bethe formula for $2Z_p v_0/v > 1$, if $a_{nl} \sim a_0$. Note that in the above analysis we have used unperturbed electron wavefunctions, which is valid only for $v \gg v_0$.

While a number of smart semi-empirical ways to improve the first Born approximation were developed [76]–[78], the rigorous approaches to improve the Bethe formula are based on the eikonal approximation instead of the Born approximation [79]. The eikonal approximation is justified if $ka_{nl} > 1$, where k is the projectile particle wave vector $k = Mv/\hbar$, and the projectile kinetic energy is large compared to the potential energy interaction with the target. For heavy projectile particles with mass much larger than the electron mass, these conditions are well satisfied. The ionization cross-section in the eikonal approximation is given by [29]

$$\sigma = 2\pi \int \frac{q\ {\rm d}q}{k^2} |f(\mathbf{q})|^2, \tag{52}$$

where $f(\mathbf{q})$ is the amplitude of ionization with momentum transfer $\mathbf{q}$

$$f(\mathbf{q}) = \frac{k}{2\pi {\rm i}} \int \rho\ {\rm d}\rho \langle {\rm final}| \exp\left(\frac{{\rm i}\int V\ {\rm d}z}{\hbar} - {\rm i}\mathbf{q}\cdot\rho \right) |{\rm initial}\rangle. \tag{53}$$

The eikonal approximation in equations (52) and (53) accounts approximately for all orders of the perturbation series, whereas the Born approximation only make use of the first order. The calculations in the eikonal approximation yield a formula similar to equation (51) [81]. Note that the validity of the eikonal approximation in equation (53) is limited to $v \gg v_0$, because the electron wavefunctions Ψ_i and Ψ_f are assumed to be unperturbed atomic functions. The influence of the projectile on the electron wavefunctions has to be taken into account for $v \lesssim v_0$. This is typically performed in the distorted wave approximation [16].

Therefore, the correction to the Born approximation in equation (51) and the eikonal approximation give a formula similar to equation (41) but with a factor $\alpha\sqrt{Z_p}$ (α is a coefficient of order unity), instead of $\sqrt{(Z_p+1)/2}$. At large velocities, both formulae give similar results.

3.2. Behaviour of cross-sections at small projectile velocities $v < v_{nl}$

If the projectile velocity is small compared with the orbital velocity, the collision is adiabatic and the electron circulates many times around both nuclei. The electronic energy states need to be determined in such a quasi-molecule as a function of the positions of both nuclei at a particular time. In both the quantum mechanical and the classical approaches, ionization is only possible if during the collision the initial and final electronic terms cross at some instant. In classical mechanics this corresponds to the so-called '$v/2$ mechanism'. In a collisional system comprised of two nuclei of equal charges (say ionization of hydrogen by a proton), an electron which is exactly in between the two nuclei experiences a very small electric field because the electric fields from both nuclei exactly cancel for all times at this point. The electron can 'ride' this saddle point of the potential if its velocity is equal to one-half the velocity of the projectile. The collision dynamics is illustrated in figure 9.

From figure 9 one can see that the electron is stranded in between the protons at $t = 15a_0/v_0$ and its velocity projection on the x-axis is one-half of the projectile velocity. A small variation of the initial condition from $z = -1.606756a_0$ (solid line) to $z = -1.606751a_0$ (dotted line) completely changes the result of the collision. After the collision the electron stays near the first nucleus and does not become ionized. As a result, the probability of ionization is extremely small even though the projectile velocity is not small (for the conditions in figure 9, $v = 1/2$ in atomic units). The mechanism for ionization described above is also so-called T-promotion in quantum-mechanical descriptions [83].

Another mechanism for ionization is attributed to the so-called S-promotion mechanism [83]. It is associated with the special type of trajectory of the electron in the field of two positive charges, shown in figure 9(c). Figure 9(c) shows that an electron with particular initial conditions tends to spiral with a large number of turns enclosing a segment of the straight line joining the nuclei figure 9(c) [84]. Such a trajectory is unstable—a small variation of initial conditions results in a completely different trajectory as shown in figure 9(c). Analysis of the electron motion in the field of two positive charges, Z_T and Z_P, which are separated by a distance R is best described in elliptical coordinates

$$\xi = \frac{r_p + r_T}{R}, \qquad \eta = \frac{r_p - r_T}{R}, \tag{54}$$

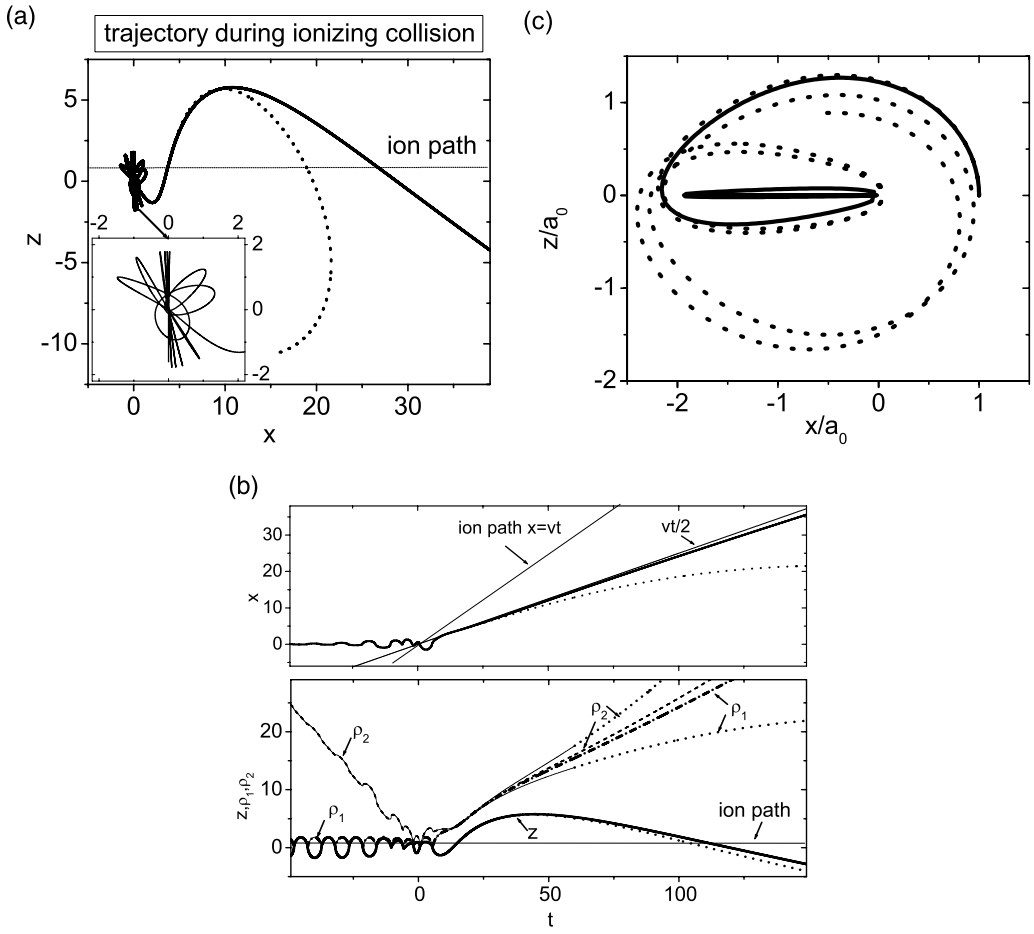

Figure 9. The trajectory of a $v/2$ collision is shown in (a) and (b). The initial conditions correspond to a hydrogen atom with total energy $-1/2$, and at $t = -60$ $x = 0 = y$, $v_x = 0 = v_y$, $z = -1.606756$ (———) and $z = -1.606751$ (· · · · · ·). The projectile moves along $z = 1$ with velocity $= 1/2$. Atomic units are used: velocity is normalized to v_0; distance is normalized to a_0; and time is normalized to a_0/v_0. Panel (b) shows the position $[x(t), z(t)]$ of the electron as a function of time, and the distance between the electron and the first (ρ_1) and the second proton (ρ_2) for the same conditions as in figure (a). The trajectory of a S-promotion is shown in figure (c) for fixed positive charges ($v \to 0$). The initial conditions correspond to an internuclear separation $2a_0$ (in atomic units); initial position of the electron $z = 0$, $x = 1$; and initial velocity $v_x = 0$, $v_z = 1.155$ (———), and $v_z = 1.165$ (· · · · · ·).

where r_p and r_T are the distances from the electron to the projectile and target nuclei, respectively. Making use of atomic units, the classical trajectory in terms of the variables ξ and η can be expressed as [84]

$$\frac{\mathrm{d}\xi}{\mathrm{d}t} = \frac{4(\xi^2 - 1)P_\xi}{R^2(\xi^2 - \eta^2)}, \qquad \frac{\mathrm{d}\eta}{\mathrm{d}t} = -\frac{4(\eta^2 - 1)P_\eta}{R^2(\xi^2 - \eta^2)}, \tag{55}$$

where the canonical momentums P_ξ and P_η are

$$P_\xi = \left(-\tfrac{1}{2}R^2|E| + \frac{(Z_P + Z_T)R\xi - \lambda}{\xi^2 - 1} - \frac{P_\phi^2}{(\xi^2-1)^2} \right)^{1/2}, \tag{56}$$

$$P_\eta = \left(-\tfrac{1}{2}R^2|E| + \frac{(Z_P - Z_T)R\eta + \lambda}{1 - \eta^2} - \frac{P_\phi^2}{(1-\eta^2)^2} \right)^{1/2}. \tag{57}$$

Here $E < 0$ is the total energy of the electron, $P_\phi = \xi\eta\, \mathrm{d}\phi/\mathrm{d}t$ is the rotational momentum around the straight line joining the nuclei, and λ is the integral of motion (for stationary nuclei)

$$\lambda = M^2 - \frac{R^2}{4}\left(P_\zeta^2 + \frac{P_\phi^2}{\zeta^2} \right) + R(Z_P \cos\theta_P + Z_T \cos\theta_T). \tag{58}$$

Here, ζ is the closest distance from the electron to the straight line joining the nuclei; P_ζ is the vector dot product of the electron momentum with the ζ-axis; $M^2 = (\mathbf{r} \times \mathbf{p})^2$ is the total rotational momentum; and θ_P and θ_T are the angles between $\mathbf{r}_p$ and $\mathbf{R}$, and $\mathbf{r}_T$ and $-\mathbf{R}$, respectively. Moreover, $\mathbf{r}_p$ is the radius vector from the projectile to the electron; $\mathbf{r}_T$ is the radius vector from the target nucleus to the electron; and $\mathbf{R}$ is the radius vector from the projectile to the target nucleus. The canonical momentum P_ξ in equation (56) tends to infinity if $\xi \to 1$, preventing the electron from approaching a segment of the straight line joining the nuclei, $\xi = 1$. In the special case

$$(Z_P + Z_T)R = \lambda, \qquad P_\phi = 0, \tag{59}$$

the singularity vanishes at the point $\xi = 1$ in equation (56). As a result, for initial conditions satisfying the condition in equation (59), P_ξ is finite for $\xi = 1$. From equation (55), ξ approach unity exponentially with time—the limiting electron trajectory lies on the internuclear axis—as shown in figure 9(c), where the initial conditions for the solid line correspond to the condition in equation (59). A small departure from the condition in equation (59) shown by the dotted line in figure 9(c) prevents the trajectory from approaching $\xi = 1$. Thus the internuclear axis $\xi = 1$, represents the locus of points of unstable equilibria. In a quantum-mechanical treatment, such periodic unstable trajectories is responsible for S-promotion of electron to the continuum (ionization) when the nuclei approach each other [85]. The potential barrier in equation (56) increases when R decreases. As a result, an electron near the top of the barrier slows down and is then collected and promoted to the continuum as the top of the barrier further rises. Due to the strong instability of the locus, a numerical simulation of the corresponding classical trajectory is extremely difficult. (We could not present the classical analogue of the ionization scenario for S-promotion, in contrast to the T-promotion as shown in figure 9(a) and (b).)

The probability of ionization is greatly enhanced in quantum mechanics due to tunnelling into classically forbidden regions of phase space. The cross-sections can be calculated using the quasi-classical method, where the probability of transition is given by

$$P(\rho) = \exp\left(-\frac{2}{\hbar}\mathrm{Im}(S) \right), \tag{60}$$

where

$$S(\rho, \epsilon) = \sum_n \int_c p \, \mathrm{d}R. \tag{61}$$

Here, $S(\rho, \epsilon)$ is the classical action of the projectile ion, and $p = \sqrt{2M(\epsilon - U(R, \rho) - E_i)}$ is the projectile momentum, generalized to classically forbidden regions of phase space where p is complex [29]. The integration contour in equation (60) is in the complex R plane around the branch points (R_n^c) where the initial and final electronic terms cross $[E_f(R_n^c) = E_i(R_n^c)]$. Moreover, n numerates different branch points or channels of ionization for S and T-promotions. The resulting cross-section for hydrogen ionization by collision with a proton is [83]

$$\sigma_{\text{adiabatic}}(v) = \pi v \sum_n R_n^2 \mathrm{e}^{-2\Delta_n/v}, \tag{62}$$

where n labels many different channels, and the coefficients Δ_n and R_n are of order unity in atomic units (R_n is determined by the branch points R_{cn}). In the range of projectile velocities $v = 0.4$–1, we find that equation (62) can be approximated to within 10% accuracy by only two exponents with $R_1 = 1.9$, $\Delta_1 = 0.53$ (corresponding to S-promotion) and $R_2 = 6.7$, $\Delta_2 = 1.8$ (corresponding to T-promotion). Because $\Delta_1 \ll \Delta_2$, primarily the S-promotion determines the ionization cross-section at small velocities ($v < 0.5$), while both mechanisms contribute to ionization for v in the range $v = 0.5$–1. Recent experimental study and quantum-mechanical calculations using the CDW-EIS model [88] show that a electron emission spectrum is dominated by a well-defined electron capture to continuum (S-promotion) peak although existence of saddle-point electron emission (T-promotion) is not confirmed.

The new fit predicts an extremely small cross-section at very low velocity $\sigma_{\text{fit}}^{\text{low-energy}}(v) \sim \exp(-1/v^2)$, whereas equation (62) gives $\sigma_{\text{adiabatic}}(v) \sim \mathrm{e}^{-1.0/v}$. The comparison of experimental data for ionization of hydrogen from [43] at low projectile velocity is shown in figure 10. At low velocity $v < 0.5$, experimental data can be fitted by $\sigma(v) \approx 0.26\pi \exp(-0.92/v)$ (in atomic units). As evident from figure 10, the numerical fit in equation (39) underestimates the cross-section for $v < 0.5$, but gives a result close to the sum in equation (62) for v in the range $v = 0.5$–1.

Numerical fit is compared with the experimental data for the ionization of He shown in figures 5(c) and (d). Adiabatic theory results are absent for helium, but the experimental ionization cross-section of He by protons can be described by equation (62) with different coefficients Δ_n and R_n. The behaviour of the experimental ionization cross-section of He by He^{2+} is somewhat puzzling because of the very slow decrease of the cross-section for small projectile velocity.

In view of these observations, the applicability of the new fit is limited to $v/[v_{nl}\sqrt{(Z_p + 1)}] > 0.5$. Note that for small projectile velocity the ionization cross-section is ten times smaller than the maximum of the cross-section, $\sigma_{\max}$, and the ionization cross-section is completely dominated by charge exchange, whose cross-section is comparable to $\sigma_{\max}$. Consequently, both experimental measurements and theoretical simulations are very difficult for very small projectile velocity.

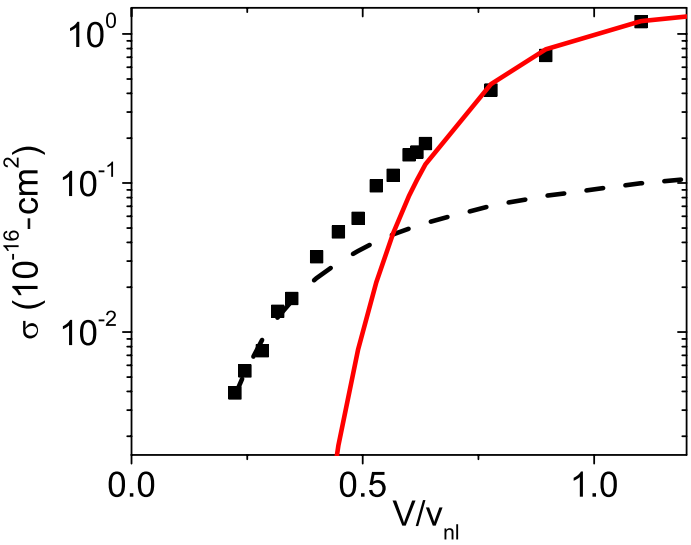

Figure 10. Comparison of experimental data for ionization of hydrogen by protons (symbols) with exponential fit $\sigma = A\exp(-2\Delta/v)$ (dashed line) and general fit formula in equation (39) (solid red line).

4. Formulary for ionization cross-section

For reference purposes a formulary of ionization cross-sections has been prepared and is presented in this section. In the high energy limit of fast projectile motion $v \gg v_{nl}$, the classical mechanical calculation can be readily carried out (see appendix A).

4.1. Calculations based on classical mechanics

4.1.1. The Bohr formula. The Bohr formula [35] neglects the electron velocity in the atom completely and is based on $v \gg v_{nl}$ limit, which gives

$$\sigma^{\text{Bohr}}(v, I_{nl}, Z_p) = 2\pi Z_p^2 a_0^2 \frac{v_0^2 E_0}{v^2 I_{nl}}. \tag{63}$$

4.1.2. Modification of the Bohr formula due to taking into account a finite electron velocity in the target. Accounting for the electron velocity gives an additional factor of $5/3$ compared with the Bohr formula. This gives the classical mechanical ionization cross-section in the limit of high projectile velocity $v \gg v_{nl}$

$$\sigma^{\text{high-energy}}_{\text{classical}}(v, I_{nl}, Z_p) = \tfrac{5}{3} 2\pi Z_p^2 a_0^2 \frac{v_0^2 E_0}{v^2 I_{nl}}. \tag{64}$$

4.1.3. General case $v \sim v_{nl}$. In the general case with $v \sim v_{nl}$, the classical mechanical calculation accounting for the finite electron velocity in the atom, but neglecting the influence

of the target nucleus on the electron has been performed by Gerjuoy [36] (see appendix A). This gives

$$\sigma^{\mathrm{GGV}}(v, I_{nl}, Z_p) = \pi a_0^2 E_0^2 \frac{Z_p^2}{I_{nl}^2} G^{\mathrm{GGV}}\left(\frac{v}{\sqrt{2I_{nl}/m_e}}\right). \tag{65}$$

The tabulation of the function $G^{\mathrm{GGV}}(x)$ is presented in [38] for $x > 1$, and in [39] for $x < 1$, which gives

$$G^{\mathrm{GGV}}(x) = \left\{ \begin{array}{ll} g(x)/4x^2 & \text{for } x > 1, \\ \dfrac{0.696}{\exp\left(\dfrac{0.585 - x}{0.096}\right) + 1} & \text{for } x < 1 \end{array} \right\}, \tag{66}$$

where

$$g(x) = \left\{ \begin{array}{l} \dfrac{35}{6} + \dfrac{35}{3\pi}\arctan c + \dfrac{128\left(x^3 b^3 - b^{3/2}\right)}{9\pi} + \dfrac{bc}{3\pi}\left(35 - \dfrac{58b}{3} - \dfrac{8b^2}{3}\right) \\ + \dfrac{2abx}{3\pi}\left[\left(5 - 4x^2\right)\left(3a^2 + 1.5ab + b^2\right) - cx\,(7.5 + 9a + 5b)\right] \\ - \dfrac{16}{\pi} x a^4 \ln(4x^2 + 1) - ax^2\left(1 + \dfrac{2\arctan c}{\pi}\right)\left(2.5 + 3a + 4a^2 + 8a^3\right) \end{array} \right\}, \tag{67}$$

and

$$a = 1/(1 + x^2), \qquad c = 3x/4, \qquad b = 1/(1 + c^2). \tag{68}$$

This calculation does not account for electron circulation around the nucleus and grossly overestimates the cross-sections for $v < \sqrt{Z_p} v_{nl}$. At large projectile velocities, quantum-mechanical effects become important, because ionization occurs mainly at large impact parameters with small momentum transfer, where ionization cannot occur according to classical mechanics. As a result, equation (65) underestimates the cross-section at large projectile velocities $v > 5v_{nl}$.

4.1.4. The Gryzinski formula. Gryzinski's approximation for the ionization cross-section [21] expressed in the form of equation (65) is given by

$$\sigma^{\mathrm{Gryz}}(v, I_{nl}, Z_p) = \pi a_0^2 E_0^2 \frac{Z_p^2}{I_{nl}^2} G^{\mathrm{Gryz}}\left(\frac{v}{\sqrt{2I_{nl}/m_e}}\right), \tag{69}$$

where

$$G^{\mathrm{Gryz}}(x) = \left\{ \begin{array}{ll} \dfrac{\alpha^{3/2}}{x^2}\left[\alpha + \dfrac{2}{3}(1 + \beta)\ln(2.7 + x)\right](1 - \beta)\left(1 + \beta^{1+x^2}\right), & \text{for } x > 0.206, \\ \frac{4}{15}x^4, & \text{for } x < 0.206, \end{array} \right. \tag{70}$$

and $\alpha = x^2/(1+x^2)$ and $\beta = 1/[4x(1+x)]$. Gryzinski made use of an artificial electron distribution function to enhance the cross-section value at large projectile velocity. Therefore for $v > v_{nl}$ the Gryzinski formula can be viewed as a fit to the Bethe formula. For $v < v_{nl}$, this formula uses a rather arbitrary behaviour $\sim v^4$. Similar to Gerjuoy's calculation, the Gryzinski formula does not account for electron circulation around the nucleus and grossly overestimates cross-sections for $v < \sqrt{Z_p} v_{nl}$.

4.2. Quantum-mechanical calculation in the Born approximation

In the general case with $v \sim v_{nl}$, the ionization cross-section in the Born approximation was first calculated in [52]. We have developed the following fit formula for the Bates and Griffing result

$$\sigma_{\text{fit}}^{\text{BA}}\left(\tilde{v} = \frac{v}{v_{nl}}\right) = 4\pi a_{nl}^2 \frac{v_0^2}{v_{nl}^2}\frac{Z_p^2}{\tilde{v}^2}[0.283\ln(\tilde{v}^2+1)+1.26]\exp\left[-\frac{1.95}{\tilde{v}(1+1.2\tilde{v}^2)}\right]. \tag{71}$$

This formula does not account correctly for electron circulation around the nucleus and grossly overestimates the cross-sections for $v < \sqrt{Z_p} v_{nl}$.

4.2.1. Bethe's asymptotic quantum-mechanical calculation in the Born approximation for $v \gg v_{nl}$. Bethe's asymptotic quantum-mechanical calculation in the Born approximation can be expressed as [40]

$$\sigma^{\text{Bethe}} = 4\pi a_0^2 \quad \frac{v_0^4 Z_p^2}{v^2 v_{nl}^2} \cdot \left[0.57\ln\left(\frac{v}{v_{nl}}\right) + 1.26\right]. \tag{72}$$

The region of validity of the Born approximation and, hence, the Bethe formula is [29, 30]

$$v > \max(2Z_p v_0, v_{nl}). \tag{73}$$

The first inequality in equation (73) assures that the projectile potential is taken into account in the Born approximation; the second inequality allows use of the unperturbed atomic wavefunction.

To describe the behaviour of the cross-section near the maximum value, the second-order correction in the parameter v_{nl}/v has been calculated in [49], yielding the cross-section in the form

$$\sigma_{\text{mod}}^{\text{Bethe}}(\tilde{v}) = 4\pi a_{nl}^2 \frac{v_0^2}{v_{nl}^2}\frac{Z_p^2}{\tilde{v}^2}\left[0.566\ln\left(\tilde{v}\right) + 1.26 - 0.66\frac{1}{\tilde{v}^2}\right], \tag{74}$$

where

$$\tilde{v} = \frac{v}{v_{nl}} = \frac{v}{\sqrt{2I_{nl}/m_e}}, \qquad a_{nl}^2 = a_0^2 \frac{E_0}{2I_{nl}}. \tag{75}$$

This modification slightly improves the Bethe formula near the maximum of cross-section, but has the same region of validity as the Bethe formula.

4.2.2. The Bethe formula for relativistic particles. The Bethe cross-section valid for relativistic particles [41] is given by

$$\sigma_{rel}^{\text{Bethe}} = 4\pi a_{nl}^2 \frac{v_0^2}{v_{nl}^2} \frac{v_{nl}^2 Z_p^2}{v^2} \left\{ M_{\text{ion}}^2 [2\ln(\gamma_p \beta_p) - \beta^2] + C_{\text{ion}} \right\}, \tag{76}$$

where $\beta_p = v_p/c$, c is the speed of light, $\gamma_p = 1\Big/\sqrt{1-\beta_p^2}$, and M_{ion}^2 and C_{ion} are characteristic constants depending on the ionized atom or ion. For the hydrogen atom, $M_{\text{ion}}^2 = 0.283$ and $C_{\text{ion}} = 4.04$.

4.3. Semi-empirical fits

4.3.1. Gillespie's fit. Gillespie's fit for the ionization cross-sections [51] is given by

$$\sigma^{\text{Gill}} = \exp\left[-\lambda_{nl} \left(v_0 \sqrt{Z_p}/v \right)^2 \right] \sigma_{\text{mod}}^{\text{Bethe}}, \tag{77}$$

where λ_{nl} is a characteristic constant of the ionized atom or ion (for example, for the ground state of atomic hydrogen, $\lambda_{nl} = 0.76$), and $\sigma_{\text{mod}}^{\text{Bethe}}$ is the modified Bethe cross-section defined in equation (74). This formula requires a knowledge of the fitting coefficients λ_{nl}, and underestimates the cross-section in the adiabatic region $v < 0.5 v_{nl}$.

4.3.2. The Olson scaling. The Olson scaling [54] for the total electron loss cross-section σ^{el}, which includes both the charge exchange cross-section σ^{ce} and the ionization cross-section, is given by

$$\sigma^{\text{el}}(v, Z_p) = \pi a_0^2 Z_p A_{nl} f^{\text{Olson}} \left(\frac{v}{v_0 \gamma_{nl} \sqrt{Z_p}} \right), \tag{78}$$

where $f(x)$ describes the scaled cross-sections

$$f^{\text{Olson}}(x) = \frac{1}{x^2} \left[1 - \exp\left(-x^2\right) \right],$$

and γ_{nl} and A_{nl} are constants. For example, $\gamma_{\text{H}} = \sqrt{5/4} = 1.12$ and $A_{\text{H}} = 16/3$ for atomic hydrogen, whereas $\gamma_{\text{He}} = 1.44$ and $A_{\text{He}} = 3.57$ for helium. However, the additional tunnelling effect not accounted in classically trajectory method can be important for very small velocities [80] and leads to a logarithmic dependence of the electron capture cross-sections at low ion velocities $v/(v_0\sqrt{Z_p}) \ll 0.2$.

4.3.3. Rost and Pattard fit formula. Rost and Pattard [58] proposed a fit for the ionization cross-section, which utilizes two fitting parameters, namely the maximum value of the cross-section and the projectile energy corresponding to the maximum value of the cross-section. They showed that if both the cross-section and the projectile velocity are normalized to the values of the cross-section and the projectile velocity at the cross-section is maximum, then the scaled cross-section $\sigma/\sigma_{\text{max}}$ is well described by the fitting function [58]

$$\sigma(v) = \sigma_{\text{max}} \frac{\exp(-v_{\text{max}}^2/v^2 + 1)}{v^2/v_{\text{max}}^2}, \tag{79}$$

where σ_{max} is the maximum cross-section, which occurs at the velocity v_{max}.

4.3.4. New scaling and fit formula. A scaling has been developed in [24], where it is shown that for ionization by a bare projectile, the values $\sigma_{\max}$ and $v_{\max}$ are well defined by the projectile charge Z_p, with

$$\sigma_{\max} = \pi a_0^2 B_{nl} \frac{Z_p^2}{(Z_p+1)} \frac{E_0^2}{I_{nl}^2}, \tag{80}$$

$$v_{\max} = v_{nl}\sqrt{Z_p+1}, \tag{81}$$

where the coefficient B_{nl} depends weakly on the projectile charge. For example, for the ionization of hydrogen by protons, $B_{nl} = 0.8$, and for the ionization of hydrogen by bare nuclei of helium or lithium, $B_{nl} = 0.93$.

Equation (79) describes well the cross-sections at small and intermediate energies, but underestimates the cross-section at high energies, because it does not reproduce the logarithmic term of the Bethe formula in equation (72). To improve the agreement with the experimental data and the Bethe formula, we propose the new scaling

$$\sigma^{\text{ion}}(v, I_{nl}, Z_p) = \pi a_0^2 \frac{Z_p^2}{(Z_p+1)} \frac{E_0^2}{I_{nl}^2} G^{\text{new}}\left(\frac{v}{v_{nl}\sqrt{Z_p+1}}\right), \tag{82}$$

where

$$G^{\text{new}}(x) = \frac{\exp(-1/x^2)}{x^2}[1.26 + 0.283\ln(2x^2+25)]. \tag{83}$$

In all previous equations, the cross-section are given per electron in the orbital. If N_{nl} is the number of electrons in the orbital, the ionization cross-section of any electron in the orbital should be increased by the factor N_{nl}. This formula underestimates the cross-section in the adiabatic region $v < 0.5v_{nl}$, where the ionization cross-sections are exponentially small $\sim \exp(-2\Delta v_0/v)$.

4.3.5. Adiabatic scaling for cross-section for $v \ll v_{nl}$. In the region of projectile velocities $v \ll v_{nl}$, an adiabatic scaling for the cross-section was proposed in [87]

$$\sigma(v, Z_p) = Z_p A \pi a_0^2 \frac{v}{v_{nl}} f_z(Z_p) \exp\left[-\frac{c v_{nl}}{v f_z(Z_p)}\right], \tag{84}$$

where $f_z(Z_p) = (1+\lambda)/(1+\lambda Z_p^{1/4})$, and A, c and λ are constants. For example, for hydrogen ionization $A = 0.96$, $c = 1.71$ and $\lambda = 0.275$. In [64, 65] it was shown that experimental data for the ionization of hydrogen and helium can be described by the scaling law in the range $0.6 < v/v_{nl}Z_p^{1/4} < 1.5$ for $Z_p \gg 1$

$$\sigma(v, Z_p)/Z_p = A\pi a_0^2 \left(\frac{v}{v_{nl}Z_p^{1/4}}\right) \exp\left[-\frac{c v_{nl} Z_p^{1/4}}{v}\right], \tag{85}$$

where $v_{nl} = \sqrt{2I_{nl}/E_0}$, and $A = 115$, $c = 7.9$ for helium.

Finally, it should be noted that a number of other semi-empirical models have been developed, which use up to ten fitting parameters to describe the ionization cross-sections over the entire projectile energy range [19].

5. Conclusions

A formulary of ionization cross-sections has been presented and widely used approximations have been tested against available experimental data for the ionization cross-sections of hydrogen, helium and lithium by numerous highly charged ion species. The limitations of the theoretical approaches have been discussed, and the regions of validity of different formulae and fits have been identified.

It was shown that scaling of [24] for the ionization cross-sections of atoms and ions by fully stripped projectiles describes well available experimental data. This scaling does not have any fitting parameters and describes the shape of the cross-section as a single function of the scaled projectile velocity (equation (39)). Note that previous scaling laws either used fitting parameters [51, 58] or actually did not match experiments in a wide range of projectile velocities [36, 21]. The proposed scaling formula agrees well with theoretical predictions in the limit of large projectile velocities. The new scaling has been verified by comparison with available experimental data and theoretical simulations for the ionization cross-sections of hydrogen, helium and lithium by numerous highly charged ion species. The agreement between the new proposed scaling and experimental data is very good. The difference between the proposed fit and the experimental data is within 15% accuracy, which is similar to the estimated uncertainty in the measurements. The validity of the fit is limited at very small velocities, where the ionization cross-section is very small, about one-tenth of the maximum cross-section $\sigma_{\max}$, and the ionization cross-section is completely dominated by charge exchange, whose cross-section is comparable to $\sigma_{\max}$. Finally, the fit is valid for scaled projectile velocity $v > 0.5 v_{nl}\sqrt{Z_p + 1}$, where $v_{nl} = v_0\sqrt{2I_{nl}/E_0}$ is the orbital velocity of the electron estimated from the ionization potential I_{nl}, where $E_0 = 27.2\,\mathrm{eV}$ (twice the hydrogen ionization potential). Similarly, the fit is valid for $E > 12.5(Z_p + 1)I_{nl}/E_0$ in units of keV amu^{-1}, where E is the projectile kinetic energy per nucleon.

Acknowledgments

This research was supported by the US Department of Energy Office of Fusion Energy Sciences and the Office of High Energy Physics.

Appendix A. Classical cross-section averaged over atomic electron velocity directions

Gerjuoy averaged the Rutherford cross-section over all orientations of the electron velocity $\mathbf{v}_e$ (for a fixed electron speed v_e) and derived the differential cross-section $\mathrm{d}\sigma/\mathrm{d}\Delta E(v_e, v, \Delta E)$ for energy transfer ΔE in the collision between a free electron and the projectile [36]. The total cross-section is calculated by integrating over values of energy transfer larger than the ionization potential ($\Delta E > I_{nl}$) and averaging over the EVDF $f(v_e)$. This gives

$$\sigma(v, I_{nl}, Z_p) = Z_p^2 \int_0^\infty \sigma_{I_{nl}}(v, v_e) f(v_e)\, \mathrm{d}v_e, \tag{A.1}$$

where

$$\sigma_{I_{nl}}(v, v_e) = \int_{I_{nl}}^\infty \frac{\mathrm{d}\sigma}{\mathrm{d}\Delta E}(v, v_e, \Delta E)\, \mathrm{d}\Delta E, \tag{A.2}$$

and $\mathrm{d}\sigma/\mathrm{d}\Delta E(v_e, v, \Delta E)$ is defined by [36]

$$\frac{\mathrm{d}\sigma}{\mathrm{d}\Delta E}(v, v_e, \Delta E) = \frac{\pi a_0^2}{4}\frac{E_0^2}{\Delta E^3}\frac{S(v, v_e, \Delta E)}{v^2 v_e}, \tag{A.3}$$

where

$$S(v, v_e, \Delta E) = \left[\begin{array}{c} \left(v^2 - v_e^2\right)\left(v_e^2 - v^2 - 2\Delta E/m_e\right)\left(v_{\mathrm{low}}^{-1} - v_{\mathrm{up}}^{-1}\right) \\ +2\left(v_e^2 + v^2 + \Delta E/m_e\right)\left(v_{\mathrm{up}} - v_{\mathrm{low}}\right) - 1/3\left(v_{\mathrm{up}}^3 - v_{\mathrm{low}}^3\right) \end{array}\right]. \tag{A.4}$$

Here, v_{up} and v_{low} are defined by

$$v_{\mathrm{up}} = v_e + v, \tag{A.5}$$

$$v_{\mathrm{low}} = \max\left(|v_e - v|, \sqrt{v_e^2 - 2\Delta E/m_e} - v\right). \tag{A.6}$$

For very large projectile velocities $v \gg v_e$, it follows that $S \approx 8v_e\left(2v_e^2/3 + \Delta E/m_e\right)$, and equation (A.3) yields

$$\frac{\mathrm{d}\sigma_{\mathrm{classical}}^{\mathrm{high-energy}}}{\mathrm{d}\Delta E}(v, v_e, \Delta E) = 2\pi a_0^2\frac{E_0^2}{\Delta E^3 m_e v^2}\left(\frac{2m_e v_e^2}{3} + \Delta E\right). \tag{A.7}$$

Substitution of equation (A.9) into equation (A.2), and subsequent substitution of equation (A.2) and the EVDF equation (9) into equation (A.1) give

$$\sigma_{\mathrm{classical}}^{\mathrm{high-energy}}(v, I_{nl}, Z_p) = \tfrac{10}{3}\pi Z_p^2 a_0^2\tfrac{v_0^2 E_0}{v^2 I_{nl}}. \tag{A.8}$$

In the general case with $v \sim v_e$, substituting the EVDF equation (9) into equations (A.2) and (A.1) yields

$$\sigma_{\mathrm{classical}}(v, I_{nl}, Z_p) = \pi a_0^2 E_0^2\frac{Z_p^2}{I_{nl}^2}G_{\mathrm{classical}}\left(\frac{v}{\sqrt{2I_{nl}/m_e}}\right), \tag{A.9}$$

where

$$G_{\mathrm{classical}}(x) = \frac{1}{x^2}\int_0^\infty\int_{1/2}^\infty \frac{S(x\sqrt{2I_{nl}/m_e}, v_e, \Delta E)\, f\,(v_e)}{\Delta E^3 v_e}\mathrm{d}\Delta E\mathrm{d}v_e. \tag{A.10}$$

The approximate formula for $G_{\mathrm{classical}}(x)$ is given above in equation (66).

Appendix B. The Born approximation

Although the Born approximation is valid only for large projectile velocities $v \gg Z_p v_0$ [29], the Born approximation does give results close to the experimental data even outside its validity range [52]. Therefore, we have studied cross-sections in the Born approximation for the entire velocity range.

In the Born approximation, the ionization cross-section for hydrogen atoms by impact of fully stripped projectile atoms with charge Z_p is given by [16, 40, 41],

$$\sigma_{nl}^{\mathrm{BA}}(v) = 8\pi a_0^2 Z_p^2 \frac{v_0^2}{v^2} \int_0^\infty \frac{P_{I_{nl}}(q, v)}{q^3}\, \mathrm{d}q, \tag{B.1}$$

where $P_{I_{nl}}(q, \tilde{v})$ is the probability of ionization, and $qm_e v_0$ is the momentum transfer during the collision. We introduce the velocity in atomic units $\tilde{v} \equiv v/v_0$, and $P_{I_{nl}}(q, \tilde{v})$ is determined by [40]

$$P_{I_{nl}}(q, \tilde{v}) = \int_0^\infty \frac{\mathrm{d}P(q, \kappa)}{\mathrm{d}\kappa} \Theta\left(q - \left(\frac{I_{nl}}{E_0} + \tfrac{1}{2}\kappa^2\right)/\tilde{v}\right) \mathrm{d}\kappa. \tag{B.2}$$

Here, $\Theta(x)$ is the Heaviside function, and $\mathrm{d}P(q, \kappa)/\mathrm{d}\kappa$ is the differential probability of ejecting an electron with momentum $\kappa m_e v_0$ when the momentum transfer from the projectile is $qm_e v_0$,

$$\frac{\mathrm{d}P(q, \kappa)}{\mathrm{d}\kappa} = \left|\left\langle \Psi_\kappa^*(\mathbf{p})\Psi_0(\mathbf{p}+\mathbf{q})\right\rangle\right|^2 = \left|\left\langle \Psi_\kappa^*(\mathbf{r})\mathrm{e}^{\mathrm{i}\mathbf{q}\mathbf{r}}\Psi_0(\mathbf{r})\right\rangle\right|^2. \tag{B.3}$$

In equation (B.3), $\Psi_\kappa^*(\mathbf{p})$ and $\Psi_\kappa^*(\mathbf{r})$ are the wavefunctions of the continuous spectrum (ionized electron) in momentum space and coordinate space, respectively; $\Psi_0(\mathbf{p})$ and $\Psi_0(\mathbf{r})$ are the wavefunctions of the ground state, and star (*) denotes complex conjugate. According to [40],

$$\frac{\mathrm{d}P(q, \kappa)}{\mathrm{d}\kappa} = 2^8 \kappa q^2 \frac{[q^2 + \frac{1}{3}(1+\kappa^2)]\exp\{-2/\kappa \arctan[2\kappa/(1+q^2-\kappa^2)]\}}{[(q+\kappa)^2+1]^3[(q-\kappa)^2+1]^3(1-\mathrm{e}^{-2\pi/\kappa})}. \tag{B.4}$$

For $q \gg 1$, the function $\mathrm{d}P(q, \kappa)/\mathrm{d}\kappa$ has a sharp maximum at $\kappa = q$ [29]

$$\frac{\mathrm{d}P(q, \kappa)}{\mathrm{d}\kappa} = \frac{8}{3\pi} \frac{1}{[(q-k)^2+1]^3}, \tag{B.5}$$

which simply means that the entire momentum q is transferred to the ionized electron momentum κ. At small $q < 1$, $\mathrm{d}P(q, \kappa)/\mathrm{d}\kappa \sim \kappa q^2$ and the width of the function $P(q, \kappa)$ as a function of κ is of order unity in atomic units.

For large projectile velocity $v \gg v_0$, considerable simplification can be made by neglecting the electron kinetic energy $(1/2)\kappa^2$ in the argument of the Heaviside function in equation (B.2). The approximation

$$\Theta\left(q - \left(\frac{I_{nl}}{E_0} + \tfrac{1}{2}\kappa^2\right)/(vv_0)\right) \to \Theta\left(q - \frac{I_{nl}/E_0}{v/v_0}\right) \tag{B.6}$$

is referred to as the close-coupling approximation. In this case, $P(q, v)$ can be characterized by a function of one argument, $S_{\mathrm{inh}}(q)$, with

$$P_{I_{nl}}(q, \tilde{v}) = S_{\mathrm{inh}}(q)\Theta\left(q - \frac{v_0 I_{nl}}{vE_0}\right), \tag{B.7}$$

where

$$S_{\rm inh}(q) = \int_0^\infty \frac{{\rm d}P(q,\kappa)}{{\rm d}\kappa}{\rm d}\kappa. \tag{B.8}$$

The function $S_{\rm inh}(q)$ is referred to as the total ionization transition strength [51]. Substituting equation (B.6) results in artificial, additional contributions to the integral in equation (B.2) for $\kappa > \kappa_{\rm add} = \sqrt{2(qv/v_0 - I_{nl}/E_0)}$. For large projectile velocities $v \gg v_0$ and $q \gg 1$, $\kappa_{\rm add} \simeq \sqrt{2qv/v_0}$. The function ${\rm d}P(q,\kappa)/{\rm d}\kappa$ has a sharp maximum at $\kappa = q$ (see equation (B.5)). Therefore the artificial additions for $\kappa > \kappa_{\rm add}$ do not contribute to the integral if $\kappa_{\rm add} > q$, which corresponds to $q < 2v$, and the substitution in equation (B.6) is valid. In the opposite case of large projectile velocities $v \gg v_0$ but small q, it follows that $q \sim v_0 I_{nl}/(vE_0) \ll 1$, for the range of q $\kappa_{\rm add} \sim 1$, and the function ${\rm d}P(q,\kappa)/{\rm d}\kappa$ decreases rapidly for $\kappa > 1$. Therefore, the artificial additions for $\kappa > \kappa_{\rm add}$ do not contribute to the integral if $\kappa_{\rm add} > 1$. Hence, the substitution in equation (B.2) is valid for $v \gg v_0$. Figure B.1 shows plots of $P_{I_{nl}}(q,\tilde{v})$ (equation (B.2)) and $S_{\rm inh}(q)$ (equation (B.8)) for $\tilde{v} = 1$ and $\tilde{v} = 3$. At small projectile velocities $v < v_0$, the substitution in equation (B.6) produces a considerable error (see figure B.1). For repetitive calculations, the function $S_{\rm inh}(q)$ in equation (B.8) can be approximated to within 3% accuracy by

$$S_{\rm inh}^{\rm app}(q) = \left[\begin{array}{ll} \dfrac{0.545q^2}{(q-0.9)^2+1.21} & q < 2 \\ \tanh(0.8q) & q \geqslant 2 \end{array}\right]. \tag{B.9}$$

The functions $S_{\rm inh}(q)$ (equation (B.8)) and $S_{\rm inh}^{\rm app}(q)$ (equation (B.9)) are shown in figure B.1.

Having estimated the function $P_{I_{nl}}(q,\tilde{v})$, the total cross-section can be evaluated analytically for large $v \gg v_0$. The region of small q contributes significantly to the cross-section (see equation (B.1)). Therefore, we split the integration in equation (B.1) into the two regions $q < q_{\rm up}$ and $q > q_{\rm up}$, where $q_{\rm up} = 1/2$. In the first region $q < q_{\rm up}$, it follows that $P_{I_{nl}}(q,v) \approx S_{\rm inh}^{\rm app}(q) \approx 0.283q^2$, and the integration in equation (B.1) gives

$$\int_0^{q_{\rm up}} {\rm d}q \frac{P_{I_{nl}}(q,v)}{q^3} \approx \int_{q_{\rm min}}^{q_{\rm up}} {\rm d}q \frac{0.283}{q} = 0.283\ln(q_{\rm up}/q_{\rm min}), \tag{B.10}$$

where $q_{\rm min} = v_0 I_{nl}/vE_0$. In the second region, only the range of $q_{\rm up} < q < 2$ contributes to the integral, because at large $q \gg 1$, $P_{I_{nl}}(q,v)/q^3 \approx 1/q^3$ and the contribution to the integral for large q quickly decreases to zero. At very large $q > 2v$, $P_{I_{nl}}(q,v)$ became smaller than unity, but this region does not contribute to the integral and can be neglected. As a result, the integral $\int_{q_{\rm up}}^\infty {\rm d}q\ P_{I_{nl}}(q,v)/q^3$ does not depend on v (for the large v under consideration). The integration from $q_{\rm up}$ to infinity gives $\int_{q_{\rm up}}^\infty {\rm d}q\ P_{I_{nl}}(q,v)/q^3 \approx 0.666$, and finally the result is similar to the Bethe formula in equation (12) with

$$\sigma^{\rm Bethe}(\tilde{v}) = 8\pi a_0^2 \frac{Z_p^2}{\tilde{v}^2}[0.283\ln(\tilde{v}) + 0.666]. \tag{B.11}$$

The small differences from the Bethe formula are due to utilization of the close-coupled approximation in equation (B.10), which overestimates $P_{I_{nl}}(q,v)$ at small q, see figure B.1.

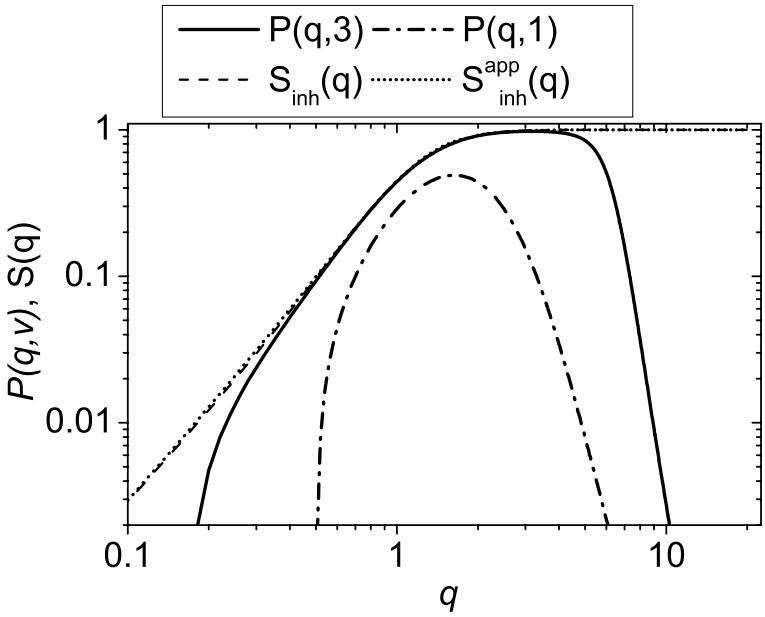

Figure B.1. Total ionization transition strength for atomic hydrogen as a function of transferred momentum q. The exact function $P(q, v)$ (equation (B.2)) for $\tilde{v} = 1$ and $\tilde{v} = 3$ is compared with the approximate function $S_{\rm inh}(q)$ (equation (B.8)) (which is independent of v) and the fit $S^{\rm app}_{\rm inh}(q)$ in equation (B.9).

Comparison with the exact calculation (figure 1) shows that the Bethe asymptotic result is close to the exact calculation in equation (B.1) for $\tilde{v} > 2$. To extend the Bethe formula to lower velocities, the second-order correction in the parameter v_0/v has been calculated in [49], yielding the cross-section in the form

$$\sigma^{\rm Bethe}_{\rm mod}(\tilde{v}) = 4\pi a_0^2 \frac{Z_p^2}{\tilde{v}^2}\left[0.57\ln\left(\tilde{v}\right) + 1.26 - 0.66\frac{1}{\tilde{v}^2}\right], \tag{B.12}$$

where $\tilde{v} = v/v_0$. Equation (B.12) agrees with the exact calculation in equation (B.1) to within 10% for $\tilde{v} > 1.1$. We have developed the following fit for the cross-section in the Born approximation,

$$\sigma^{\rm BA}_{\rm fit}(\tilde{v}) = 4\pi a_0^2 \frac{Z_p^2}{\tilde{v}^2}[0.283\ln(\tilde{v}^2+1) + 1.26]\exp\left[-\frac{1.95}{\tilde{v}(1+1.2\tilde{v}^2)}\right], \tag{B.13}$$

which agrees with the exact calculation in equation (B.1) to within 2% for $\tilde{v} > 1$, and to within 20% for $0.2 < \tilde{v} < 1$.

The previous analysis was performed for the hydrogen atom. In the case of hydrogen-like electron orbitals, the similarity principle can be used. The quantity $\mathrm{d}P(q,\kappa)/\mathrm{d}\kappa$ is identical for different electron orbitals if q, κ are scaled with the factor $1/Z_T = v_0/v_{nl}$ [29]. Therefore, $P_{nl}(q, v) = P_H(qv_0/v_{nl}, v/v_{nl})$, where H denotes the hydrogen atom, and

$$\sigma^{\rm BA}_{\rm fit}\left(\tilde{v} = \frac{v}{v_{nl}}\right) = 4\pi a_0^2 \frac{v_0^4}{v_{nl}^4}\frac{Z_p^2}{\tilde{v}^2}[0.283\ln(\tilde{v}^2+1) + 1.26]\exp\left[-\frac{1.95}{\tilde{v}(1+1.2\tilde{v}^2)}\right], \tag{B.14}$$

where

$$\tilde{v} = \frac{v}{v_{nl}} = \frac{v}{\sqrt{2I_{nl}/m_e}}. \tag{B.15}$$

As we have noted for helium, most scalings can be used even for non-hydrogen-like electron orbitals, provided the relationship in equation (B.15) is used.

B.1. Comparison between the quantum-mechanical and classical trajectory calculations for $v \gg v_{nl}$

We have previously noted that the classical trajectory calculation underestimates the ionization cross-section at large velocities $v \gg v_{nl}$. To compare the ionization cross-section calculated in the classical trajectory and Born approximations, we present both cross-sections in the form of equation (B.1). In the limit $v \gg v_{nl}$, the momentum transferred to the electron during a collision with impact parameter ρ is given by equation (1), i.e.,

$$q_x(\rho) \equiv m_e \Delta v_x(\rho) = \frac{2e^2 Z_p}{v\rho}, \tag{B.16}$$

where x-axis is chosen in the direction perpendicular to the projectile ion trajectory along the momentum transfer. Because $v \gg v_{nl}$, the electron velocity is neglected in equation (B.16). In classical mechanics, ionization occurs if the energy transfer to the electron is more than the ionization potential, $[(m_e\mathbf{v}_e + \mathbf{q})^2 - m_e^2 v^2]/2m_e > I_{nl}$.

A small momentum transfer to the electron along the projectile trajectory $q_z(\rho)$ can be determined making use of the energy conservation. Due to conservation of the momentum, the momentum transferred from the projectile particle is $-q_z(\rho)$. The projectile energy change is $[(M\mathbf{v} - \mathbf{q})^2 - M^2 v^2]/2M = -vq_z$. Conservation of energy gives

$$vq_z \equiv \frac{1}{2m_e}[(m_e\mathbf{v}_e + \mathbf{q})^2 - m_e^2 v_e^2]. \tag{B.17}$$

In the limit $v \gg v_e$, it follows that $q_z \ll q_x$, and consequently the total transferred momentum to the electron is $q = \sqrt{q_{\mathbf{x}}^2 + q_z^2} \simeq q_x$. The momentum of the ejected electron can be determined from the energy conservation relation

$$\kappa^2/2m_e = [(m_e\mathbf{v}_e + \mathbf{q})^2 - m_e^2 v_e^2]/2m_e - I_{nl}. \tag{B.18}$$

In classical mechanics, the ionization probability of the ejected electron with momentum κ in a collision with total momentum transfer q is given by the integral over the electron distribution function,

$$\frac{\mathrm{d}P_c(q,\kappa)}{\mathrm{d}\kappa} = \frac{\kappa}{m_e}\int f(\mathbf{v}_e)\,\mathbf{dv}_e\,\delta\left(\frac{\kappa^2}{2m_e} - q_x v_x - \frac{q^2}{2m_e} - I_{nl}\right). \tag{B.19}$$

Introducing the one-dimensional electron distribution function

$$f_x(v_{\mathrm{ex}}) = \int f(\mathbf{v}_e)\,\mathrm{d}v_y\,\mathrm{d}v_z, \tag{B.20}$$

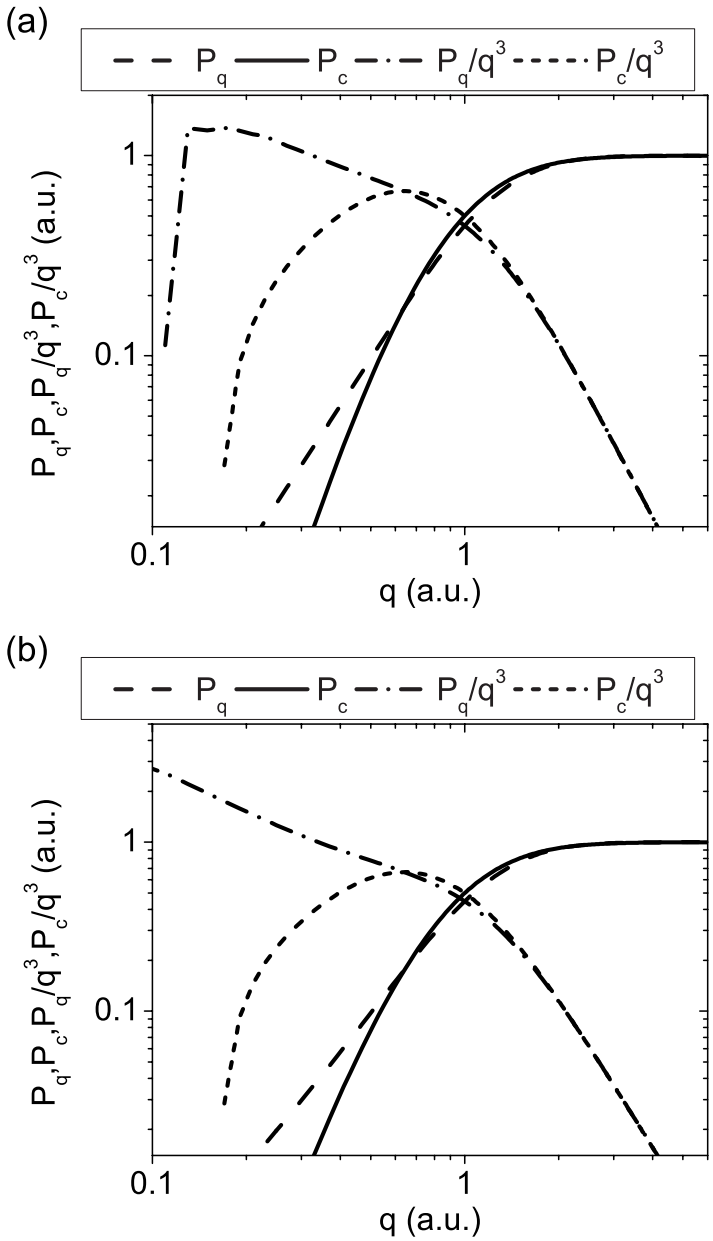

Figure B.2. Probability of ionization of atomic hydrogen as a function of transferred momentum; $P_c(q)$ is given by classical mechanics (equation (B.30)), and $P_q(q, v)$ is given by quantum mechanics (equation (B.2)). The plots correspond to (a) $\tilde{v} = 5$ and (b) $\tilde{v} = 15$.

and substituting $q \simeq q_x$, equation (B.19) simplifies to become

$$\frac{\mathrm{d}P_c(q,\kappa)}{\mathrm{d}\kappa} = \frac{\kappa}{qm_e} f_x\left(\frac{\kappa^2 - q^2 - 2m_e I_{nl}}{2qm_e}\right). \tag{B.21}$$

For hydrogen-like electron orbitals given by equation (9), $f_x(v_{\rm ex})$ can be readily calculated to be

$$f_x\left(v_{\rm ex}\right) = \frac{8}{3\pi}\frac{v_{nl}^5}{[v_{\rm ex}^2 + v_{nl}^2]^3}. \tag{B.22}$$

Substituting the hydrogen-like electron distribution function equation (B.22) into equation (B.29) gives in atomic units

$$\frac{{\rm d}P_c(q,\kappa)}{{\rm d}\kappa} = \frac{16\kappa}{3\pi}\frac{(2qm_e)^5 v_{nl}^5}{[(\kappa^2 - q^2 - 2m_e I_{nl})^2 + (2qm_e v_{nl})^2]^3}. \tag{B.23}$$

Let us compare equation (B.23) with the quantum-mechanical result equation (B.5). In the limit $q \gg 1$, $\kappa \approx q$ and the two functions are equivalent. Both functions ${\rm d}P(q,\kappa)/{\rm d}\kappa$ have a maximum at $\kappa = q$, and the width of the maximum is of order 1, which simply means that the entire momentum q is transferred to the ionized electron momentum κ.

Moreover, it is possible to prove that the classical mechanical ${\rm d}P_c(q,\kappa)/{\rm d}\kappa$ is equivalent to the quantum-mechanical function ${\rm d}P_q(q,\kappa)/{\rm d}\kappa$ for any s-electron orbital (spherically symmetrical wavefunction). Indeed, for large $k \gg 1$, the ejected electron can be described as a sum over plane waves $\Psi_\kappa^*(\mathbf{r}) \approx {\rm e}^{{\rm i}\mathbf{kr}}$, and substituting $\Psi_\kappa^*(\mathbf{r})$ into equation (B.3) gives

$$\frac{{\rm d}P_q(q,\kappa)}{{\rm d}\kappa} = \frac{1}{(2\pi\hbar)^3}\int \left|\left\langle {\rm e}^{{\rm i}(\mathbf{q}-\mathbf{k})\mathbf{r}/\hbar}\Psi_0(\mathbf{r})\right\rangle\right|^2 k^2 {\rm d}o_{\mathbf{k}} = \frac{1}{m_e^3}\int f\left(\frac{\mathbf{q}-\mathbf{k}}{m_e}\right) k^2 {\rm d}o_{\mathbf{k}}, \tag{B.24}$$

where integral over ${\rm d}o_{\mathbf{k}} = 2\pi\sin\vartheta{\rm d}\vartheta$ designates averaging over all directions of the $\mathbf{k}$-vector, ϑ is the angle between $\mathbf{q}$ and $\mathbf{k}$, and $f(v_e)$ is the electron distribution function in velocity space. Note that $|\mathbf{q}-\mathbf{k}|^2 = \mathbf{q}^2 + \mathbf{k}^2 - 2\mathbf{q}\cdot\mathbf{k} = (q-k)^2 + 4qk\sin\vartheta/2^2$. In the limit $q \gg 1$, $k \approx q$ and only small ϑ contribute to the integral in equation (B.24). Therefore, averaging over all directions of the $\mathbf{k}$-vector gives

$$\frac{1}{m_e^2}\int f\left(\frac{\mathbf{q}-\mathbf{k}}{m_e}\right) k^2 {\rm d}o_{\mathbf{k}} = \frac{1}{m_e^2}\int f\left(\frac{\sqrt{(q-k)^2 + qk\vartheta^2}}{m_e}\right) 2\pi k^2\vartheta\ {\rm d}\vartheta. \tag{B.25}$$

Introducing $v_\perp = k\vartheta/m_e$, the integral in equation (B.25) takes form

$$\int f\left(\sqrt{\left(\frac{q-k}{m_e}\right)^2 + v_\perp^2}\right){\rm d}^2 v_\perp = f_x\left(\frac{q-k}{m_e}\right), \tag{B.26}$$

where f_x is the one-dimensional EVDF. Substituting equations (B.26) and (B.25) into equation (B.24) yields

$$\frac{{\rm d}P_q(q,\kappa)}{{\rm d}\kappa} = \frac{1}{m_e} f_x\left(\frac{q-k}{m_e}\right). \tag{B.27}$$

Note that in the limit $q \gg m_e v_{nl}$, it follows that $\kappa \approx q$, and equation (B.21) becomes

$$\frac{{\rm d}P_c(q,\kappa)}{{\rm d}\kappa} = \frac{1}{m_e} f_x\left(\frac{q-k}{m_e}\right). \tag{B.28}$$

Finally, comparing equations (B.27) and (B.28) we arrive at the equivalence of functions $\mathrm{d}P(q,\kappa)/\mathrm{d}\kappa$ in quantum mechanics and classical mechanics in the limit $q \gg m_e v_{nl}$.

The situation is completely different for small $q \ll m_e v_{nl}$. From equation (B.23) it follows that $\mathrm{d}P_c(q,\kappa)/\mathrm{d}\kappa \sim \kappa q^5$, and $\mathrm{d}P_c(q,\kappa)/\mathrm{d}\kappa$ is much smaller than $\mathrm{d}P_q(q,\kappa)/\mathrm{d}\kappa \sim \kappa q^2$. *Therefore, classical mechanics strongly underestimates the probability of ionization for small transferred momentum* $q < m_e v_{nl}$.

The total probability of ionization in classical mechanics is

$$P_c(q) = \int_0^\infty \mathrm{d}\kappa \frac{\mathrm{d}P_q(q,\kappa)}{\mathrm{d}\kappa} = \int \Theta\left(q v_{\mathrm{ex}} + \frac{q^2}{2m_e} - I_{nl}\right) f(\mathbf{v}_e)\,\mathbf{dv}_e. \tag{B.29}$$

Equation (B.29) simplifies to become

$$P_c(q) = \int \Theta\left(q v_{\mathrm{ex}} + \frac{q^2}{2m_e} - I_{nl}\right) f_x(v_{\mathrm{ex}})\,\mathrm{d}v_{\mathrm{ex}}. \tag{B.30}$$

The differential cross-section for momentum transfer q is given by

$$\mathrm{d}\sigma_c(q) = 2\pi\rho(q)\mathrm{d}\rho(q), \tag{B.31}$$

where $\rho(q)$ is given by equation (B.16). Substituting $\rho(q)$ from equation (B.16) into equation (B.31) gives

$$\mathrm{d}\sigma_c(q) = \frac{8\pi e^4 Z_p^2}{v^2 q^3}\mathrm{d}q, \tag{B.32}$$

which is the Rutherford differential cross-section for scattering at small angles. Finally, the total ionization cross-section is

$$\sigma_c = 8\pi a_0^2 Z_p^2 \frac{v_0^2}{v^2}\int_{I_{nl}/v}^\infty \frac{P_c(q)}{q^3}\mathrm{d}q. \tag{B.33}$$

In equation (B.33), we accounted for the fact that the minimum q is $q = I_{nl}/v$. Note that in the region $q = [1-3]I_{nl}/v$ ionization occurs due the collisions with very fast electrons $v_e \sim v \gg v_{nl}$, and $q_x \sim q_z$. The previous analysis which assumed $v_e \ll v$ and $q_x \gg q_z$ is not valid in this region of extremely small q. However, because $P_c(q)/q^3 \to 0$ as $q \to 0$, this region of $q = [1-3]I_{nl}/v$ does not contribute to the integral in equation (B.33) and can be neglected. Moreover such small momentum transfers correspond to very large impact parameter $\rho/v \sim a_{nl}/v_{nl}$, where the collision becomes adiabatic. Therefore, accurate calculations yield even smaller $P_c(q)$ than in equation (B.30).

Equation (B.33) is identical to equation (B.1), where the quantum-mechanical ionization probability $P_q(q,v)$ is replaced by the classical mechanical ionization probability $P_c(q)$ in equation (B.30). The functions $P_q(q,v)$ (equation (B.2)) and $P_c(q)$ (equation (B.30)) are shown in figure B.2. Figure B.2 shows that the functions $P_{I_{nl}}(q,v)$ and $P_c(q)$ are nearly identical for $q > 0.6$. The classical probability of ionization $P_c(q)$ rapidly tends to zero for $q < 0.6$, while the quantum probability of ionization, $P_q(q) \approx 0.283q^2$, is much larger than $P_c(q)$ at small q. The cross-section is determined by $P_q(q)/q^3$. Therefore the region of small q contributes considerably to the quantum-mechanical cross-section. Note that $P_q(q)/q^3 \to 0$ as $q \to I_{nl}/\tilde{v}$. It follows that

the region of small q contributes most to the cross-section (compare figure B.2(a) for $\tilde{v} = 5$, and figure B.2(b) for $\tilde{v} = 15$). For $\tilde{v} = 5$, the classical mechanical ionization cross-section in atomic units is $\sigma_c = 0.23$, and the quantum-mechanical ionization cross-section is $\sigma_q = 0.30$, which is 30% larger than the classical mechanical cross-section. For $\tilde{v} = 15$, $\sigma_c = 0.025$ and $\sigma_q = 0.043$, which is 70% larger.

References

[1] Logan B G *et al* 2002 *Laser Part. Beams* **20** 369
[2] Keating G M and Bougher S W 1992 *J. Geophys. Res. Space Phys.* **97** 4189
[3] Beyer H, Shevelko V P (eds) 1999 *Atomic Physics with Heavy Ions* (Berlin: Springer)
[4] Bogaerts A, Gijbels R and Carman R J 1998 *Spectrochim. Acta Part B: At. Spectrosc.* **53** 1679
[5] Stockl C *et al* 1998 *Nucl. Instrum. Methods* A **415** 558
[6] Datz S, Drake G W F, Galagher T F, Kleinpoppen H and Zu Putlitz G 1999 *Rev. Mod. Phys.* **71** S223
[7] Chen P 1987 *Part. Accel.* **20** 171
Chen P, Su J J, Katsouleas T, Qilks S and Dawson J M 1987 *IEEE Trans. Plasma Sci.* **15** 218
[8] Govil R, Leemans W P, Backhaus E Yu and Wurtele J S 1999 *Phys. Rev. Lett.* **83** 3202
[9] Rajagopalan S, Cline D B and Chen P 1995 *Nucl. Instrum. Methods* A **355** 169
[10] Tauschwitz T, Yu S S, Eylon S, Reginato L, Leemans W, Rasmussen J O and Bangerter R O 1996 *J. Fusion Eng. Des.* **32–33** 493
[11] Roth M *et al* 2001 *Phys. Rev. Lett.* **86** 436
Tabak M, Hammer J, Glinsky M E, Kruer W L, Wilks S C, Woodworth J, Campbell E M, Perry M D and Mason R J 1994 *Phys. Plasmas* **1** 1626
[12] Voronov G S 1997 *At. Data Nucl. Data Tables* **65** 1
[13] Rudd M E, Kim Y-K, Madison D H and Galallagher J W 1992 *Rev. Mod. Phys.* **64** 441
[14] Rudd M E, Kim Y-K, Madison D H and Gay T J 1985 *Rev. Mod. Phys.* **57** 965
[15] Ogurtsov G N 1972 *Rev. Mod. Phys.* **44** 1
[16] Janev R K, Presnyakov L P and Shevelko V P 1999 *Physics of Highly Charged Ions* (Berlin: Springer)
[17] McDowell M R C and Coleman J P 1970 *Introduction to the Theory of Ion–Atom Collisions* (Amsterdam: North-Holland)
[18] Bransden B H and McDowell M R C 1992 *Charge Exchange and the Theory of Ion–Atom Collisions* (Oxford: Clarendon)
[19] McDaniel E W, Mitchell J B A and Rudd M E 1993 *Atomic Collisions, Heavy Particle Projectiles* (New York: Wiley)
[20] McGuire J H 1997 *Electron Correlation Dynamics in Atomic Scattering* (Cambridge: Cambridge University Press)
[21] Gryzinski M 1965 *Phys. Rev.* A **138** 322
[22] http://webofscience.com
[23] Gillespie G 1982 *J. Phys. B: At. Mol. Phys.* **15** L729
Gillespie G 1983 *Phys. Lett.* A **93** 327
[24] Kaganovich I D, Startsev E A and Davidson R C 2004 *Phys. Plasmas* **11** 1229
[25] Mueller D, Grisham L, Kaganovich I, Watson R L, Horvat V and Zaharakis K E 2001 *Phys. Plasmas* **8** 1753
[26] Olson R E, Watson R L, Horvat V and Zaharakis K E 2003 *Phys. Rev.* A **67** 022706
[27] Watson R L, Peng Y, Horvat V, Kim G J and Olson R E 2003 *Phys. Rev.* A **67** 022706
[28] Mueller D, Grisham L, Kaganovich I, Watson R L, Horvat V, Zaharakis K E and Peng Y 2002 *Laser Part. Beams* **20** 551
[29] Landau L D and Lifshitz E M 1958 *Quantum Mechanics* (Reading, MA: Addison-Wesley)
[30] Bohr N 1948 *K Dan. Vidensk. Selsk. Mat.-Fys. Medd.* **18** N8

[31] Kaganovich I D, Startsev E and Davidson R C 2001 Evaluation of ionization cross sections in energetic ion–atom collisions *Proc. 2001 Particle Accelerator Conference* http://accelconf.web.cern.ch/AccelConf/p01/PAPERS/TPAH314.PDF
[32] Kaganovich I D *et al* 2005 *Nucl. Instrum. Methods Phys. Res.* **544** 91
[33] Kaganovich I D, Startsev E A and Davidson R C 2003 *Phys. Rev.* A **68** 022707
[34] Matsuo T *et al* 1999 *Phys. Rev.* A **60** 3000
[35] Thompson J J 1912 *Phil. Mag.* **23** 449
[36] Gerjuoy E 1966 *Phys. Rev.* A **148** 54
[37] Ponce V H 1977 *At. Data Nucl. Data Tables* **19** 63
[38] Vriens L 1966 *Proc. R. Soc. Lond.* **90** 935
[39] Scott Armel M 2000 *PhD Thesis* University of California at Berkeley; http://faculty.oxy.edu/scottfunk/Sci/index.html
[40] Bethe H 1930 *Ann. Phys. (Lpz.)* **5** 325
[41] Bethe H A and Jackiw R 1968 *Intermidiate Quantum Mechanics* 2nd edn (New York: Benjamin-Cummings)
[42] Shah M B, Elliott D S and Gilbody H B 1987 *J.Phys. B: At. Mol. Phys.* **20** 2481
[43] Shah M B, Geddes J, Mc Laghlin B M and Gilbody H B 1998 *J. Phys. B: At. Mol. Opt. Phys.* **31** L757
[44] Barnett C F (ed) 1990 Collisions of H, H2, He and Li atoms and ions with atoms and molecules *Atomic Data for Fusion* vol 1, ORNL-6086
Phaneuf R A, Janev R K and Pindzola M S (ed) 1987 Collisions of carbon and oxygen ions with electrons, H, H2 and He *Atomic Data for Fusion* vol 5, ORNL-6090 http://www-cfadc.phy.ornl.gov/redbooks
[45] Shah M B and Gilbody H B 1982 *J. Phys. B: At. Mol. Phys.* **15** 413
[46] Shah M B and Gilbody H B 1983 *J. Phys. B: At. Mol. Phys.* **16** 4395
[47] Knudsen H *et al* 1984 *J. Phys. B: At. Mol. Phys.* **17** 3545
[48] Kolakowska A, Pindzola M S and Schultz D R 1999 *Phys. Rev.* A **59** 3588
[49] Kim Y K and Inokuti M 1971 *Phys. Rev.* A **3** 665
Inokuti M 1971 *Rev. Mod. Phys.* **43** 297
[50] Shevelko V P, Tolstikhina I Yu and Stoehlker Th 2001 *Nucl. Instrum. Methods* B **184** 295
[51] Gillespie G H 1978 *Phys. Rev.* A **18** 1967
[52] Bates D R and Griffing G 1953 *Proc. Phys. Soc. Lond.* **66** 961
[53] Bohr N and Linhard J 1954 *Dan K. Vidensk. Selsk. Mat.-Fys. Medd.* **28** 1
[54] Olson R E 1978 *Phys. Rev.* A **18** 2464
Olson R E *et al* 1978 *Rev. Lett.* **41** 163
[55] Hardie D J W and Olson R E 1983 *J. Phys. B: At. Mol. Phys.* **16** 1983
[56] Janev R K 1983 *Phys. Rev.* A **18** 1810
[57] Stolterfoht N, DuBois R D and Rivarola R D 1997 *Electron Emission in Heavy Ion–Atom Collisions* (Berlin: Springer)
[58] Rost J M and Pattard T 1997 *Phys. Rev.* A **55** R5
[59] Shah M B and Gilbody H B 1985 *J. Phys. B: At. Mol. Phys.* **18** 899
[60] Shah M B, McCallion P and Gilbody H B 1989 *J. Phys. B: At. Mol. Opt. Phys.* **22** 3037
[61] Schlachter A S *et al* 1981 *Phys. Rev.* A **23** 2331
[62] Be S H *et al* 1986 *J. Phys. B: At. Mol. Phys.* **19** 1771
[63] Dubois R D and Toburen L H 1988 *Phys. Rev.* A **38** 3960
[64] Wu W *et al* 1995 *Phys. Rev. Lett.* **75** 1054
[65] Wu W *et al* 1996 *Phys. Rev.* A **53** 2367
[66] Datz S *et al* 1990 *Phys. Rev.* A **41** 3559
[67] Berg H, Ullrich J and Bernstein E 1992 *J. Phys. B: At. Mol. Opt. Phys.* **25** 3655
[68] Illescas C and Riera A 1999 *Phys. Rev.* A **60** 4546
[69] Fainstein P D, Ponce V H and Rivarola R D 1991 *J.Phys. B: At. Mol. Phys.* **24** 3091
[70] Shah M B, Elliott D S and Gilbody H B 1985 *J. Phys. B: At. Mol. Phys.* **18** 4245

[71] DuBois R D 1985 *Phys. Rev.* A **32** 3319
[72] Fiori M R, Jalbert G, Bielschowsky C E and Cravero W 2001 *Phys. Rev.* A **64** 012705
[73] Haugen H K, Andersen L H, Hvelplund P and Knudsen H 1982 *Phys. Rev.* A **26** 1950
[74] Gilespie G 1981 *Phys. Rev.* A **24** 608
[75] Knudsen H and Reading J F 1992 *Phys. Rep.* **212** 107
[76] Theodosiou C E 1988 *Phys. Rev.* A **38** 4923
[77] Theodosiou C E 1987 *Phys. Rev.* A **36** 2067
[78] Sander W and Theodosiou C E 1990 *Phys. Rev.* A **42** 5208
[79] McGuire J H 1982 *Phys. Rev.* A **26** 143
[80] Duman E L, Men'shikov L I and Smirnov B M 1979 *Sov. Phys.—JETP* **49** 260
[81] Matveev V I, Pazdzerkii V A and Rakhimov Kh Yu 2001 *Tech. Phys.* **46** 512
[82] Olson R E 1983 *Phys. Rev.* A **27** 1871
[83] Ovchinnikov S Y 1990 *Phys. Rev.* A **42** 3865
[84] Abramov D I, Ovchinnikov S Y and Solov'ev E A 1990 *Phys. Rev.* A **42** 6366
[85] Ovchinnikov S Y and Macek J H 1995 *Phys. Rev. Lett.* **75** 2474
[86] Ovchinnikov S Y, Macek J H, Gordeev Y S and Ogurtsov G N 2003 Ionization dynamics in atomic collisions *Many-Particle Quntum Dynamics in Atomic and Molecular Fragmentation* ed J Ulrich and V P Shevelko (Berlin: Springer)
[87] Janev R K, Ivanovski G and Solov'ev E A 1994 *Phys. Rev.* A **49** R645
[88] Nesbitt B S *et al* 2000 *J. Phys. B: At. Mol. Opt. Phys.* **33** 637
[89] Irby V D 1989 *Phys. Rev.* A **39** 54
[90] Santos A C F and Dubois R D 2004 *Phys. Rev.* A **69** 042709